의학박사 학위논문

Development of polymorphism independent translocator protein (TSPO)-targeting positron emission tomography using [^{18}F]CB251 in acute neuroinflammation models

급성 신경 염증 모델에서 [^{18}F]CB251 을 이용한 유전자다형성 비의존성 전이체단백질 표적 양전자단층촬영술 개발

2021 년 02 월

서울대학교 대학원
의과학과 의과학전공
김 경 민

A thesis of the Degree of Doctor of Philosophy

급성 신경 염증 모델에서 [^{18}F]CB251 을 이용한 유전자다형성 비의존성 전이체단백질 표적 양전자단층촬영술 개발

Development of polymorphism independent translocator protein (TSPO)–targeting positron emission tomography using [^{18}F]CB251 in acute neuroinflammation models

February, 2021

The Department of Biomedical Science,
Seoul National University
College of Medicine
Kyungmin Kim

Development of polymorphism independent translocator protein (TSPO)-targeting positron emission tomography using [^{18}F]CB251 in acute neuroinflammation models

by
Kyungmin Kim

A thesis submitted to the Department of Biomedical Science in partial fulfillment of the requirements for the Degree of Doctor of Philosophy in Biomedical Science at Seoul National University College of Medicine

February, 2021

Approved by Thesis Committee:

Professor Jae Min Jeong Chairman
Professor Keon Hwa Kang Vice chairman
Professor Sin Ha Park
Professor Gi Jeong Cheon
Professor Seung Jun Oh

급성 신경 염증 모델에서 [^{18}F]CB251 을 이용한 유전자다형성 비의존성 전이체단백질 표적 양전자단층촬영술 개발

지도교수 강 건 욱

의학 박사 학위논문으로 제출함

2021 년 2 월

서울대학교 대학원

의과학과 의과학전공

김 경 민

김경민의 의학박사 학위 논문을 인준함

2021 년 2 월

위 원 장 정재민 (인)

부위원장 강건욱 (인)

위 원 (인)

위 원 (인)

위 원 (인)

ABSTRACT

Introduction: Neuroinflammation is the inflammation of central nervous system, which acts as a protective reaction, but excessive inflammation provokes detrimental effects and neurological diseases. Therefore, diagnosis of neuroinflammation is important because it allows early diagnosis and prediction of neuronal diseases. The translocator protein (TSPO) has been suggested as an attractive target for detecting neuroinflammation, and several TSPO radiotracers have been developed. However, due to the problem that the binding affinity of TSPO ligands was affected by single nucleotide polymorphisms (SNP) in human TSPO gene, development of new ligands that bind TSPO regardless of SNP is still needed. Here, we visualized neuroinflammation with [^{18}F]CB251 PET which is not affected by TSPO polymorphism.

Methods: To assess binding specificity of [^{18}F]CB251 to TSPO *in vitro*, we established cells expressing TSPO wildtype gene or TSPO mutant gene (Ala → Thr at 147th amino acid; A147T). Competitive inhibition assay was performed to compare binding affinity of CB251 by TSPO polymorphism. To verify that

[^{18}F]CB251 is a radiotracer targeting TSPO, we generated the cells with different expression level of TSPO using pCMV-TSPO/eGFP or pCMV-shTSPO/eGFP vectors. The level of [^{18}F]CB251 uptake in each cells was analyzed and compared. We also compared The level of [^{18}F]CB251 uptake in non-activated and activated immune cells. Lipopolysaccharide (LPS) was intracranial injected into the right striatum of the mouse brain using a stereotaxic device to induce neuroinflammation. Saline was used as a control. Splenocytes (2×10^7) were isolated from transgenic mice with luciferase gene (B6.Luc^{Tg}), and intravenously injected to intracranial LPS mouse model (B6) for monitoring localization of peripheral immune cell with bioluminescence imaging (BLI). To detect neuro-inflammation in mouse model, [^{18}F]CB251 PET/MR scans and BLI were acquired. To determine if [^{18}F]CB251 PET signal can assess the effect of CDDO-methyl ester, an inflammatory cytokine inhibitor, CDDO-Me was treated three times in neuroinflammatory mouse model.

Results: IC_{50} ratio (TSPO A/T Mut/TSPO WT) of CB251 was 1.14, which was closed to 1. In addition, in contrast to the TSPO-targeting probe [^{18}F]PBR28, which is known to be sensitive to

TSPO polymorphisms, [^{18}F]CB251 was taken up by cells regardless of TSPO polymorphisms. [^{18}F]CB251 also showed TSPO specificity in cells expressing different levels of TSPO and activated immune cells. In intracranial LPS model, [^{18}F]CB251 radioactivity was higher in the LPS-injected right striatum of the mouse brains, which co-registered with MR signals. Bioluminescence signals of peripheral immune cells isolated from B6.Luc^{Tg} were also localized to the LPS-injected region and increased 1.48 times in the neuroinflammatory model than in the control. The anti-inflammatory efficacy of CDDO-Me on neuroinflammation was quantitatively evaluated with [^{18}F]CB251 PET/MRI.

Conclusions: These results indicated that [^{18}F]CB251 PET/MRI and BLI have great potential for diagnosis of neuroinflammation. Moreover, [^{18}F]CB251 PET targeting TSPO might be an effective method for evaluating the severity of neuroinflammation associated with neurological diseases and the response to therapy, regardless of human TSPO polymorphisms.

Keywords: neuroinflammation, translocator protein, single nucleotide polymorphism, [^{18}F]CB251 positron emission

tomography

Student number: 2014-25054

CONTENTS

LIST OF TABLES

LIST OF FIGURES

LIST OF ABBREVIATIONS

TSPO, translocator protein

LPS, Lipopolysaccharide

SNP, Single nucleotide polymorphism

TSPO A/T Mut, TSPO mutant gene (Alanine → Threonine at 147^{th} amino acid; A147T)

CNS, Central nervous system

BBB, Blood-brain barrier

GFP, Green fluorescence protein

BLI, Bioluminescence imaging

PET, Positron emission tomography

MRI, Magnetic resonance imaging

Gd-DOTA, Gadoteric acid, gadolinium 1,4,7,10-tetraazacyclododecane-N,N',N",N"'-tetraacetate

[^{18}F]fm-PBR28-d_2, [^{18}F]Fluoromethyl-PBR28-d_2

CDDO-Me, An inflammatory cytokine inhibitor, 2-cyano-3, 12-dioxooleana-1,9-dien-28-oic acid methyl ester

FBS, Fetal bovine serum

FACS, Fluorescence activated cell sorting

IHC, Immuno-histochemical staining

CHAPTER 1

Development of TSPO-targeting PET using [^{18}F]CB251 in acute neuroinflammation models

INTRODUCTION

1.1 Neuroinflammation and the role of intrinsic and migrated immune cells

Neuroinflammation is the inflammation of central nervous tissue and is initially a protective response, but excess inflammatory responses provoke detrimental effects in central nervous system (CNS). The causes of neuroinflammatory response include infection, traumatic brain injury, toxic metabolites or autoimmunity and these factors led to immune cells to migrate to the site of inflammation (1, 2). The brain was once considered as an immune-privileged organ unlike innate and adaptive immunity being closely controlled in interaction with the periphery immune system (1, 3). It was also thought that there were no bidirectional interactions between the brain and the peripheral immune systems. However, currently it has known that the brain and peripheral immune responses can communicate and influence each other in pathological conditions. Inflammatory response is mediated by pro-inflammatory mediators such as IL-6, TNF-a, nitric oxide (NO) and ROS released from immune cells (1, 4, 5). These factors act as starting point for not only activation of microglia-residential immune cells but also disruption of Blood-

Brain Barrier (BBB) and thereby promote migration of peripheral immune cells into inflammatory region. Several reports suggested that the interplay between peripheral immune system and CNS immune system may accelerate pathogenesis of various neurodegenerative diseases and allow neurodegenerative mechanisms to persist. Therefore, the attempts have been developed to image and diagnose the neuroinflammatory region, which are important for predicting neuropathology.

1.2 Strategies of indirect imaging for neuroinflammation

Until now, many imaging modalities and strategies to visualize neuroinflammation have been proposed (Table 1). Non-invasive imaging such as optical, MRI, SPECT, and PET is increasingly applied for inflammation in the CNS. [^{99m}Tc]hexamethylpropylene-amineoxime (HMPAO) SPECT is a representative method for scanning cerebral blood flow as gold standard neuropathological criteria (6, 7). Also, [^{99m}Tc]DTPA SPECT and gadolinium-DTPA MRI have been performed to target BBB disruption and change of vascular permeability (8, 9). [^{18}F]FDG PET can reflect glucose metabolic changes in disease neuronal tissue and inflammatory cells, therefore, it has been

used for imaging neuroinflammation (10). However, [^{18}F]FDG PET is difficult to use for the early diagnosis of neuronal diseases because it's low signal-to-background ratio. In addition, since these approaches incorporate the effects of various neuropathologic response, quantitative follow-up of neuroinflammation is not possible (9, 11, 12). Therefore, better imaging biomarkers still need to be developed to overcome the limitation of indirect imaging for neuroinflammation.

1.3 Strategies of leukocyte targeted imaging for neuroinflammation

Recent studies have shown that several trials for neuroinflammation targeting using phenomenon-recruited immune cells including microglia and peripheral immune cells in inflammatory region (Table 1). Many researchers have been employed specific targets of the immune cells such as metabolic enzymes, membrane markers and inflammatory cytokines in non-invasive molecular imaging techniques (9, 13). For example, VCAM1-MPIO (micron particles of iron oxide) have used for detecting VCAM1 expression on endothelial cells. VCAM1 is an adhesion molecule, which facilitate adhesion of leukocytes. Thus,

MR imaging of VCAM1-MPIO could represent neuroinflammation (14). Cyclooxygenase (COX)-1 is an important enzyme that converts arachidonic acid to prostaglandins, which is expressed in microglia cells in the brain and has been reported to be overexpressed in the inflammatory response. [^{11}C]ketoprofen, a COX-1 specific PET probe, was developed using this phenomenon (15). Cannabinoid receptor 2 (CB2) is also used as an attractive membrane marker for imaging neuroinflammation. It is expressed on microglia/macrophages and the expression level is upregulated in inflammation. Imaging activated immune cells is useful tool for assessing the severity of inflammatory response (16). So, imaging the immune cells and investigating the interactions between CNS immune cells and infiltrating peripheral immune cells are important for understanding disease progression. However, there are still need to develop better biomarkers and ligands due to poor sensitivity to specific target or low binding affinity between target and ligand.

1.4 Translocator protein (TSPO) as an attractive biomarker for neuroinflammation

Translocator protein (TSPO) is a protein located in outer mitochondrial membrane with the functions of peripheral benzodiazepine receptor as well as a cholesterol transporter. TSPO is mainly expressed within monocyte-derived cells and has been suggested as an attractive biomarker for neuroinflammation (12, 17). The reason is that human TSPO has been reported to have low expression in brain, but, is upregulated in inflammatory situations. PET studies using this characteristic have been conducted in neuronal diseases (16). In addition, recent studies have shown expression of TSPO is linked to inflammatory responses that occur after brain injury, and in some neurodegenerative diseases (17).

1.5 TSPO-targeting radiotracer, [^{18}F]CB251

Numerous indole-based TSPO ligands, cholesterol-like compounds and miscellaneous TSPO ligands have been synthesized and analyzed on their TSPO affinities (18-21). In specific, alpidem structure has been reported to act on both central and peripheral benzodiazepine receptor. For increasing TSPO selectivity, alpidem structure was preferred over other structures. Many chemists have been tried to substitute several

positions of the imidazo[1,2-a]pyridine nucleus for higher TSPO selectivity and specificity (20). Because that, many structure-activity-relationship studies have been conducted. [^{18}F]CB251, an [^{18}F] labeled alpidem analogue, was synthesized from 2-phenyl-imidazo[1,2-a]pyridine. In earlier paper (20), the synthesis of [^{18}F]CB251 and the ability to detect neuro-inflammatory regions has been reported. In this study, we tested [^{18}F]CB251 as a TSPO-targeting PET probe for the imaging of inflammatory cells in neuroinflammatory region.

1.6 The aim of this study

In chapter 1, we determine if [^{18}F]CB251 could distinguish activated immune cells and detect neuroinflammatory region in acute neuroinflammatory models. We also used bioluminescent image (BLI) to verify that peripheral immune cells isolated from spleen of luciferase-expressing transgenic mouse infiltrated into neuroinflammatory region. We demonstrated immune cell infiltration, disruption of BBB junction and confirmed the potential of [^{18}F]CB251 ligand as a promising TSPO targeting probe. Finally, we also attempted to evaluate therapeutic efficacy of an anti-inflammatory agent using [^{18}F]CB251 PET probe and

determine if [^{18}F]CB251 PET could quantitatively assess the severity of neuroinflammation.

Table 1. Characterization of several imaging strategies for neuroinflammation

	Strategies	Imaging targets	Imaging probes	Pros[b,c]	Cons[b,c]
Indirect imaging	Blood flow	Inflammatory response (Hypertension)	[^{99m}Tc]HMPAO [^{99m}Tc]ECD	Reflect physiological response of neuropathology, including neuroinflammation	Low specificity and targeting accuracy Difficult to early diagnosis
	Vascular permeability	Altered blood-brain barrier	[^{99m}Tc]DTPA Gd-DTPA		
	Glucose metabolism	Activated/migrated immune cells	[^{18}F]FDG [^{11}C]Arachidonic acid		
Leukocyte targeted imaging[a]	Leukocyte function	Oxidative stress	MPO-Gd [^{18}F]FASu	Specific and sensitive to neuroinflammation Quantitative follow-up of neuroinflammation	Different cell types and molecular mediators participate in a series of neuroinflammation Insufficient sensitivity by tracer Need to better tracer development and validation
		Proteolytic activity (MMP)	[^{18}F]CGS27023A [^{64}Cu]DOTA-CTT		
		Cox1/2	[^{11}C]ketoprofen		
		TSPO	[^{11}C]PK1195 [^{11}C]PBR28		
		CB2	[^{11}C]A836339 [^{11}C]KD2		
	Leukocyte labeling	Phagocytosis/uptake	USPIO		
	Leukocyte adhesion molecule	VCAM-1	VCAM1-MPIO		
		ICAM-1	ICAM-MPIO		
		Integrin avb3	[^{18}F]galacto-RGB [^{99m}Tc]NC100692		
		CD62	Gd-DTPA-B(sLe^x)A		

Ref. a)12, b)11, c)45

MATERIALS AND METHODS

1. Cell culture

Mouse macrophage cell line, RAW264.7 and mouse splenocytes were used to determine TSPO expression of activated immune cells. LPS (50 ng/mL, Sigma-Aldrich, St.Louis, MO, USA) and IFN-γ (20 ng/mL, Sigma-Aldrich) were incubated with immune cells for activation. To establish cells with different levels of TSPO expression, the 293FT (Invitrogen, Carlsbad, CA, USA) and MDA-MB-231 (ATCC, Manassas, VA, USA) cell lines were selected. Cells (Raw264.7, MDA-MB-231, 293FT) were cultured in DMEM with 10% FBS and 1% antibiotics (penicillin-streptomycin). 293FT cells were maintained in complete DMEM with L-Glutamate (2 mM), Sodium pyruvate (1 mM) and MEM NEAA. Splenocytes isolated from the spleens of transgenic mice with luciferase gene (C57BL/6.Luc^{Tg}, Macrogen, Seoul, Korea) were cultured in RPMI 1640 medium with 10% FBS and 1% antibiotics. All media and reagents including FBS and antibiotics for maintaining cells were purchased from Gibco (Grand Island, NY, USA).

2. Transient transfection for TSPO expression

To establish cells with different expression of the TSPO protein, the 293FT cell line and MDA-MB-231 cell line were transiently transfected with vectors (pCMV-eGFP/TSPO) (AddGene, Cambridge, MA,USA) harboring the eGFP and TSPO coding sequences or vectors (pCMV-eGFP/shTSPO; AddGene) with eGFP and TSPO shRNA coding sequences. Each vector (2.5 μg/mL) was transfected by Lipofectamine 2000 (Invitrogen, Waltham, MA, USA). Fluorescent images were acquired by a confocal microscopy (Leica TCS SP8; Wetzlar, Hesse, Germany), and verification was also performed by western blotting.

3. [^{18}F]CB251 radiochemistry

In this study, [^{18}F]fluoride-labeled CB251 probe provided by Bundang Seoul national university hospital was used for PET imaging (20). The [^{18}F]CB251 radiotracer was synthesized according to a protocol described in a previous study[19]. Briefly, [^{18}F]CB251 was acquired by a single-step radiolabeling with nucleophilic aliphatic substitution. Briefly, [^{18}F]fluoride was isolated from a ^{18}O (p,n) ^{18}F nuclear reaction by a chromafix-HCO_3 cartridge and eluted with 0.4 mL of nBu$_4$NHCO$_3$ in a 10% water/methanol solution. The solution containing [^{18}F]fluoride

was dried with 0.3 ml of acetonitrile under nitrogen stream (x 2), and then 3 mg of the tosylate-CB251 precursor were added. After the mixture was heated and cooling, it was diluted with 10 mL of water. This solution was loaded onto a C18 Sep-Pak cartridge, washed with water (10 mL) and eluted with CH_3CN (1.5 mL). The eluent was diluted with 1.5 mL water and separated by a semi-prep HPLC system equipped with UV and gamma-ray detectors. The [^{18}F]CB251 fraction was collected after 20 min, diluted with 20 mL of water, loaded onto a C18 plus Sep-Pak cartridge, and then eluted by 10% ethanol/saline to remove the HPLC solvent.

4. *in vitro* uptake with [^{18}F]CB251

Cells were plated in 6-well plates (Sigma-Aldrich) to reach approximately 80% confluency. The cells were preincubated with glucose-free RPMI1640 medium (Gibco) for 4 hours before *in vitro* uptake. Cells were trypsinized, counted and transferred to 5 mL test tube. 1×10^5 cells were suspended in the pre-warmed Hank's balanced salt solution (HBSS, Sigma-Aldrich) containing 0.5% (w/v) bovine serum albumin (BSA, Sigma-Aldrich). 0.185 MBq of [^{18}F]CB251 was added to the tubes, and

the cells were maintained in a humidified 37° C incubator with 5% CO_2 for 1 hour. The cells were washed three times with cold HBSS and radioactivity was measured by a Cobra II gamma counter (Canberra Packard; Vaughan, Ontario, Canada). The cells were then lysed for 5 min using 1% sodium dodecyl sulfate solution (total volume 200 μL, SDS, Sigma-Aldrich). Cell lysates were collected and total protein concentrations were analyzed by the BCA assay kit (Pierce, Rockford, IL, USA). Radioactivity was normalized according to the amount of total protein at the time of assay. All experiments were performed in triplicate.

5. Western blotting

Cells were lysed by RIPA lysis buffer (Sigma-Aldrich) with a protease inhibitor (Roche, Branchburg, NJ, USA) cocktail. Total protein concentrations were analyzed using a BCA protein assay kit (Pierce Endogen, Rockford, IL, USA), and proteins (20 μg) were separated on 10% polyacrylamide gels. Separated proteins on gels were then transferred to PVDF membranes (Millipore, Watford, Herts, UK), which were blocked by 5% skim milk in TBS-T solution (Tris buffered saline; 20 mM Tris, 138 mM NaCl,

and pH 7.4 with 0.1% Tween-20) for 1 hour. Membranes were incubated with following primary antibodies (4° C, O/N) and then bound HRP conjugated secondary antibodies for 1 hour. These primary antibodies were used: Rabbit anti-TSPO (Abcam, Cambridge, Cambs, UK), Rabbit anti-iNOS (Santa-Cruz Biotechnology, Santa-Cruz, CA, USA), Mouse anti-β-actin (Sigma-Aldrich). Anti-rabbit IgG (Cell Signaling Technology, Danvers, MA, USA) and anti-mouse IgG (Cell signaling) were used as secondary antibody.

6. Animal ethics

All the animal experimental designs and procedures were approved by the Institutional Animal Care and Use Committee (IACUC) of Seoul National University and followed the ethical standards of Seoul National University Hospital guidelines.

7. Isolation of splenocytes from spleen of B6. Luc^{Tg} mice

Cells expressing luciferase gene were obtained from the spleens of transgenic C57BL/6-luc^{Tg} mice. Grinded spleen was centrifuged (1300 rpm, 5 min, 4° C) and Red blood cell lysis buffer (1 mL/spleen, Sigma-Aldrich) was added to the cell pellet.

The mixture was incubated at RT for 3 min with tapping to remove red blood cells. After a double volume of RPMI medium was added to the cells, cell pellet was obtained by centrifugation. Red blood cell lysis buffer was added 2 or 3 more times until all the red blood cells were completely lysed. Cells were re-suspended with complete RPMI 1640 medium (10% FBS, 1% antibiotics) and filtered through a cell strainer (40 μm nylon, Falcon, Oneonta, NY). To verify the correlation with cell numbers and bioluminescent signals, Cells (3.175×10^5 to 5×10^6) were plated onto 24-well plates. Bioluminescent images of cells were acquired after the addition of D-luciferin (300 μg/mL, Caliper Life Science, Hopkinton, MA) to measure bioluminescent signals following luciferase activity. Bioluminescence intensity was analyzed by an IVIS 100 system (Perkin Elmer, Waltham, MA, USA). To monitor the in vivo distribution of immune cells, luciferase-expressing splenocytes (2×10^7) were adoptively transferred into recipient C57BL/6 mice.

8. Intracranial LPS mouse model

C57BL/6 mice (male, 6 weeks old) were used for the intracranial LPS inflammatory model. LPS (5 μg/2 μL, Sigma-Aldrich,

dissolved in saline) was intracranial injected to the right striatum of the mouse brain for inducing regional neuroinflammation (anteroposterior, +1.8; mediolateral, +2.0; dorsoventral, −3.0) using a robotic stereotaxic device (Stoelting, Wood Dale, IL) equipped with a Hamilton syringe at a rate of 0.25 μL/min. Saline was intracranial injected as a control (22−24).

9. [^{18}F]CB251 PET/MRI scan

PET/MR images were acquired by a simultaneous small animal PET insert (SimPET, Brightonic imaging, Seoul, Korea) combined with an M7 1.0T MRI system (Aspect Imaging, Jerusalem, Israel). To detect neuroinflammation, [^{18}F]CB251 PET/MR images were acquired 4 days after intracranial LPS injection. [^{18}F]CB251 (9.25 to 11.1 MBq per mouse) was injected intravenously 20 min before PET/MR scans. A PET/MR scan with a 30 x 30 mm field−of−view (FOV) was performed simultaneously for 40 min. To evaluate breakage of BBB, both T1− and T2−weighted MR scans were acquired for up to 4 days at 1 day interval after gadolinium (Gd−DOTA, 0.5 mmol/kg) was injected intravenously into intracranial LPS mouse model 20 min before MR scanning (20). The T1−weighted fast−spin echo

sequence consisted of a repetition time of 200 msec and an echo time of 10 msec. The T2-weighted fast spin echo sequence consisted of a repetition time of 3000 msec and an echo time of 63.84 msec. PET and MR images were reconstructed and analyzed by the AMIDE program (ver 0.9.0, http://amide.sourceforge.net).

10. *In vivo* Bioluminescence imaging

An in vivo IVIS100 imaging system (Xenogen, Alameda, CA, USA) was used to monitor luciferase-expressing peripheral immune cells. D-luciferin (3 mg/mouse) was injected intraperitoneally into intracranial LPS mouse model 10 min before optical imaging. The bioluminescent signal was acquired and analyzed by Living Image ver.2.50.2 software (Xenogen).

11. Immunohistochemistry

Brain tissues from intracranial LPS mouse were embedded in paraffin and sectioned to thickness of 4 μm segments. Heat-induced method for antigen epitope retrieval was used. Brain tissues were blocked with 3% normal serum in PBS for 30 min, and the primary antibodies were incubated overnight at 4° C.

The following primary antibodies were used; Anti-CD68, anti-CD86, anti-F4/80 (Santa Cruz Biotechnology, Santa Cruz, CA, USA), anti-CD4, anti-CD8, anti-Iba-1, and anti-TSPO (Abcam, Cambridge, UK). The brain tissues were washed with PBS three times and then incubated with biotinylated secondary antibodies (aanti-mouse IgG for CD86; anti-goat IgG for CD68; anti-rat IgG for F4/80; anti-rabbit IgG for TSPO, CD4, CD8, and Iba-1; all secondary antibodies from Santa Cruz Biotechnology. Avidin-biotin solution (Vector Laboratories, Burlingame, CA, USA) was incubated for 1 hr at RT. DAB (3, 3 -diaminobenzidine) substrate (Vector Laboratories, Burlingame, CA, USA) was used for developing the antigenic signals, according to the manufacturer's instructions. The brain tissues were then counterstained with hematoxylin and mounted with Permount Mounting solution (Thermo Fisher Scientific, Fair Lawn, NJ, USA).

12. Treatment of anti-inflammatory agent, CDDO-methyl ester (CDDO-Me)

2-Cyano-3,12-dioxo-oleana-1,9(11)-dien-28-oicacid methyl ester (CDDO-methyl ester or CDDO-Me, Sigma-

Aldrich) was dissolved in DMSO to make a 10 mM stock solution. The stock solution was further diluted with a 200 nM CDDO-Me solution using 7.5% PBST (1.5 ml Tween-20 dissolved in 20 ml PBS). Mice was treated with 100 μL of CDDO-ME solution via intraperitoneal injection once daily for 3 days beginning 1 day after intracranial administration of LPS.

13. Statistical analysis

All results were calculated as means ± standard deviation (SD). Statistically significant differences were analyzed by a paired 2-sample Student t-test. Statistical significance was considered $p<0.05$. All statistical analysis was measured using GraphPad Prism 5 software (San Diego, CA).

RESULTS

In vitro [^{18}F]CB251 uptake of the cells with different expression level of TSPO

To determine if [^{18}F]CB251 could reflect different expression levels of TSPO *in vitro*, I regulated TSPO expression level using pCMV-TSPO/eGFP for TSPO up-regulation and pCMV-shTSPO/eGFP for TSPO down-regulation (Figure 1-1). 293FT cell line which has low basal expression level of TSPO was transfected with pCMV-TSPO/eGFP. Fluorescence images showed increased green fluorescence signals. Increased TSPO expression was observed in western blot analysis. MDA-MB-231 cell line which shows high levels of TSPO was used for reducing TSPO expression by transfecting pCMV-shTSPO/eGFP. Fluorescence images also showed increased eGFP signals and decreased TSPO levels were observed in western blot (Figure 1-2). These results reflected successful transfection of each vector in the target cells. The uptake of [^{18}F]CB251 was elevated in TSPO up-regulated cells and that was reduced in TSPO down-regulated cells (Figure 1-3). These data demonstrated [^{18}F]CB251 uptake is directly regulated by the change of TSPO expression, which suggests that [^{18}F]CB251

is specific to TSPO in the cell level.

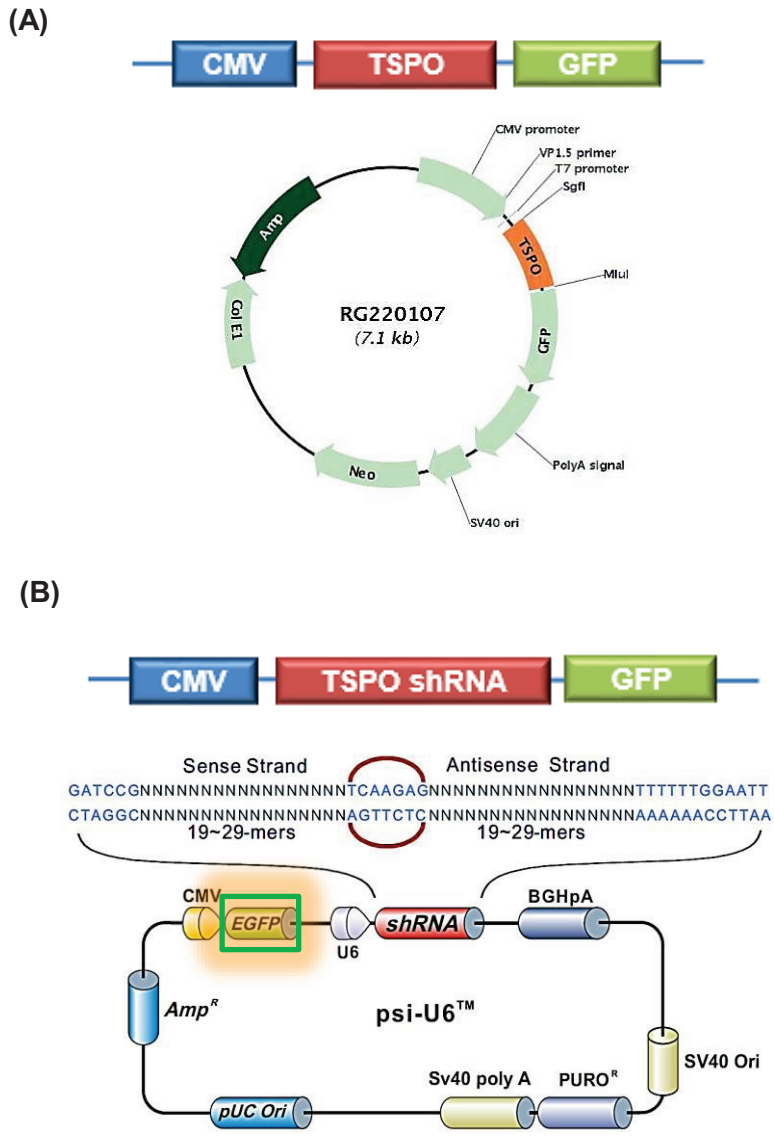

Figure 1-1. Vector constructs for regulating TSPO expression

(A) Viral vector construct for TSPO up-regulation (B) Viral vector construct for TSPO down-regulation

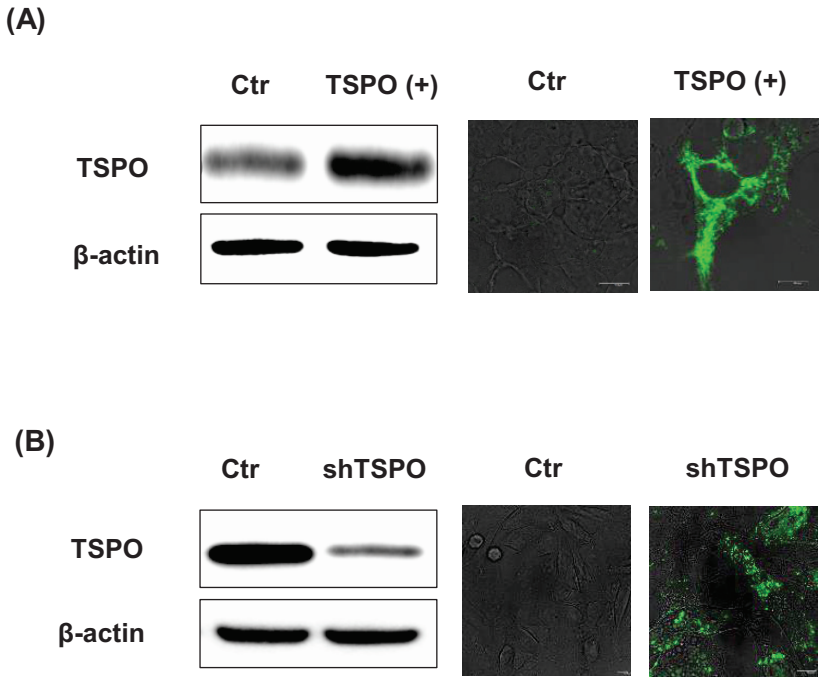

Figure 1-2. Expression of TSPO after transfection of TSPO-regulating vectors (A) Western blots and eGFP images of 293FT cells after transfection of TSPO up-regulation vector (B) Western blots and eGFP images of MDA-MB-231 cells after transfection of TSPO down-regulation vector

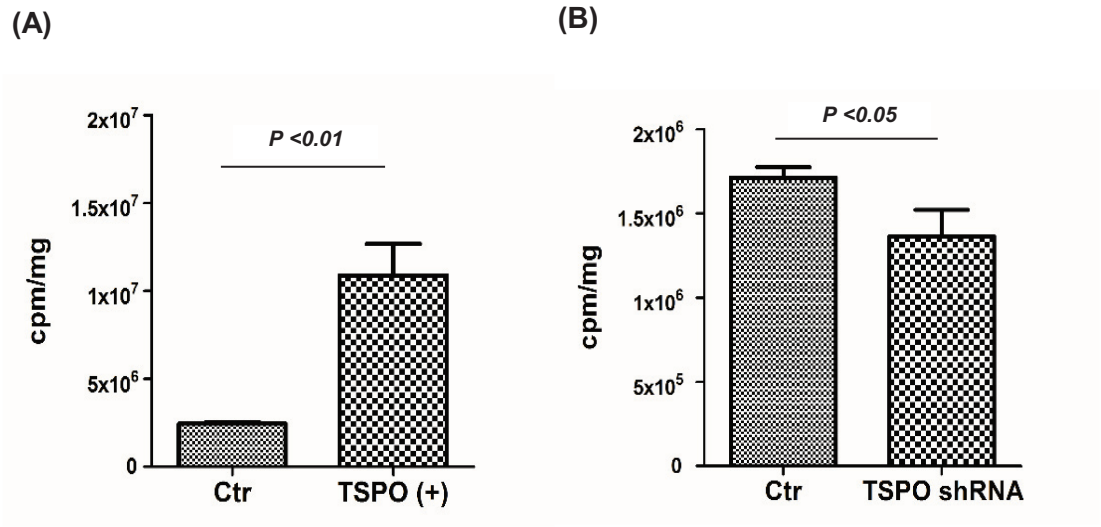

Figure 1-3. [^{18}F]CB251 uptake in different expression level of TSPO

(A) [^{18}F]CB251 uptake in TSPO over-expressing 293FT cells (cpm/mg: count per min/mg, in triplicate, n=3) (B) [^{18}F]CB251 uptake in MDA-MB-231 cells with TSPO expression downregulated by shTSPO treatment (in triplicate, n=3)

In vitro [^{18}F]CB251 uptake of activated immune cells

To test [^{18}F]CB251 could distinguish activated immune cells, [^{18}F]CB251 cellular uptake in activated macrophage cell line and peripheral immune cells from mouse spleen was conducted. RAW264.7, mouse macrophage cell line, and splenocytes with red blood cell removed were treated with LPS and IFN-r for 24 hrs. Increased TSPO expression in activated immune cells was observed in immunoblot. The expression of iNOS, known as an activated macrophage marker, was also increased in activated immune cells (Figure 1-4A). As I expected, increased uptake of [^{18}F]CB251 was consistent with increased expression of cellular TSPO in activated immune cells (Figure 1-4B). Our data indicated [^{18}F]CB251, TSPO radiotracer, has potential to distinguish the condition of immune cells, non-activated or activated state, suggesting it can be used to image inflammatory region.

(A)

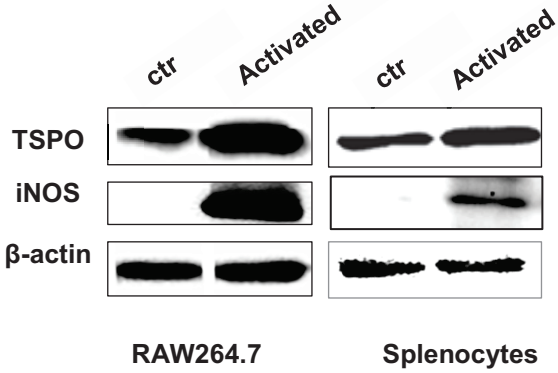
ctr
Activated
ctr
Activated
TSPO
iNOS
β-actin
RAW264.7
Splenocytes

(B)

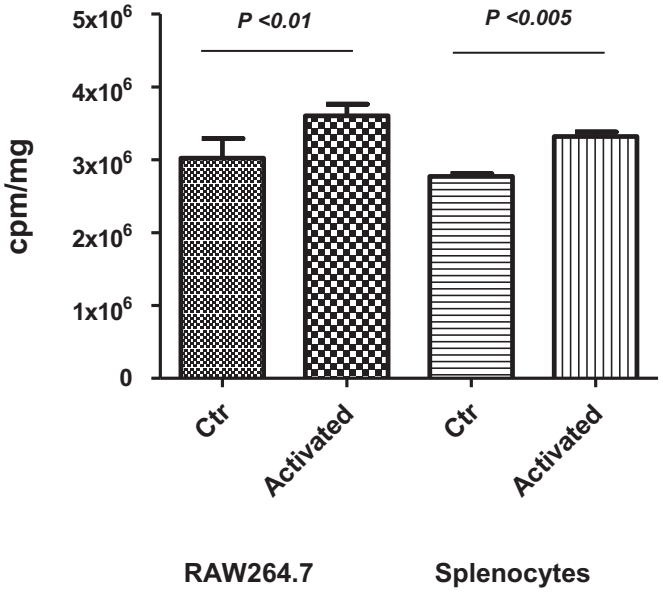
5x10^6
4x10^6
3x10^6
2x10^6
1x10^6
0
cpm/mg
P <0.01
P <0.005
Ctr
Activated
Ctr
Activated
RAW264.7
Splenocytes

Figure 1−4. [^{18}F]CB251 uptake in activated macrophage cell line and activated splenocytes (A) Western blot analysis of TSPO and iNOS according to treatment with LPS and IFN− γ in RAW264.7 macrophage cell lines and splenocytes (B) *In vitro* uptake assay of [^{18}F]CB251 in Raw264.7 cells and splenocytes showing differential TSPO expression (in triplicate, n=3)

Confirmation of luciferase signal of splenocytes

The infiltrated peripheral immune cells in the region of neuroinflammation induce prolonged inflammation and exacerbate neuronal toxicity. Therefore, imaging infiltrated peripheral immune cells provides useful information for evaluation of inflammatory response and neuronal damage to the brain. BLI has been used in several animal models because of its advantage in identifying the bio-distribution of living cells. Therefore, I isolated peripheral immune cells from spleen of luciferase-expressing transgenic mouse (C57BL/6.Luc^{Tg}). Splenocytes from B6.Luc^{Tg} included T cells, B cells and macrophages in similar proportions of splenocytes from B6 wildtype (Table 2). It has been observed that the composition and the function of immune cells of reporter Tg mouse were not different from those of wildtype mouse. BLI signals of diluted splenocytes were increased in a cell number-dependent manner and a very excellent correlation (r^2 = 0.9991) was observed (Figure 1-5). This data indicated the number and migration region of splenocytes can be evaluated *in vivo* through BLI signal.

(A)

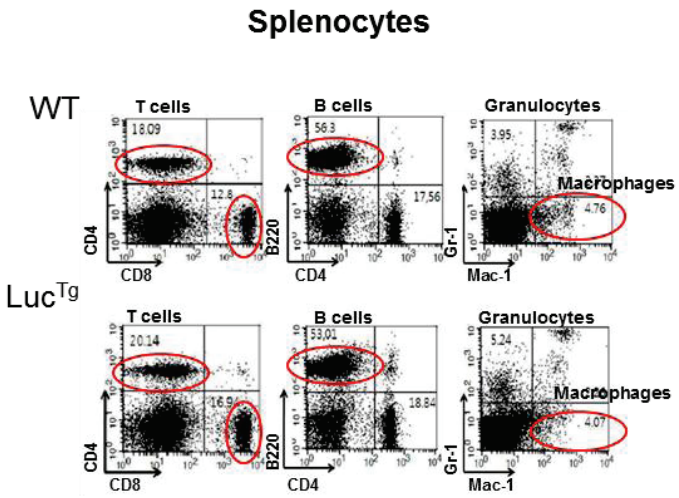

(B)

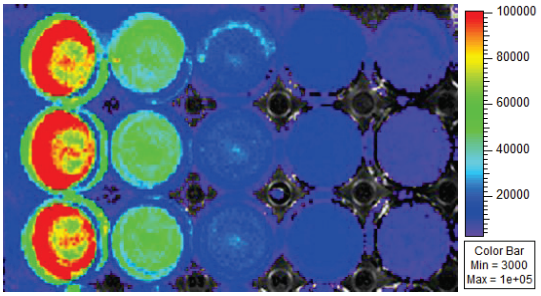

5 2.5 1.25 0.625 0.3175

(10^6 cells/well)

(C)

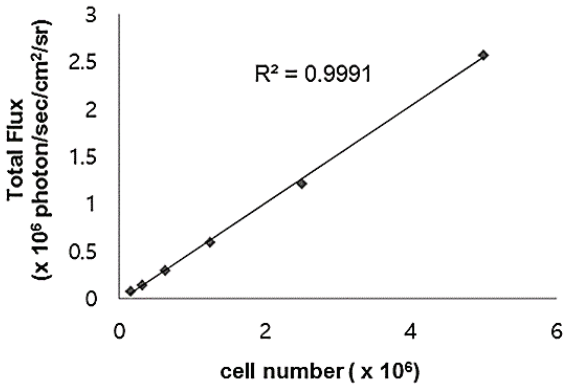

Figure 1-5. Analysis of immune cells from spleen cells of C57BL/6.Luc^{Tg} mouse (A) Flow cytometry of immune cells from C57BL/6 (wildtype) and C57BL/6.Luc^{Tg} mouse (B) Semi-quantitative analysis of luciferase-expressing immune cells by bioluminescence imaging. (C) Quantitative analysis of luciferase intensity and the number of cells by linear regression (R^2=0.9991)

Table 2. Comparison of immune cell composition in C57BL/6 and C57BL/6.Luc^{Tg} mouse spleen

Immune cells	B6 spleen	B6.Luc^{Tg} spleen
T cells	30.1%	27%
CD4+ T cells	55% of T cells	68.2% of T cells
CD8+ T cells	39.7% of T cells	25.5% of T cells
B cells	64.6%	57.2%
NK cells	1.8%	1.2%
Neutrophils (CD11b+)	0.9%	0.4%
Monocytes (CD11c+)	2.6%	1.4%
[DC cells / macrophage]	[1.7% / 0.9%]	[1.1%/ 0.3%]

Bio-distribution of luciferase expressing splenocytes in the intracranial mouse model

To monitor the distribution of immune cells in intracranial mouse model, I adoptively transferred splenocytes into two different mouse model, intracranial saline-injected mouse model and LPS-injected mouse model. Intravenous administrations of splenocytes were distributed in similar pattern in various homing organs of each mouse model except brain (Figure 1-7). Although the brain is typically not an organ in which peripheral immune cells exists, the BLI signal was observed in the brain of LPS-injected mouse. So, I found adoptive transferred splenocytes were visualized in the inflammatory region of the brain. In addition, our results indicated transferred splenocytes can be distributed in mouse and I can confirm the location and measure extent of splenocyte recruitment in each organ using BLI signal.

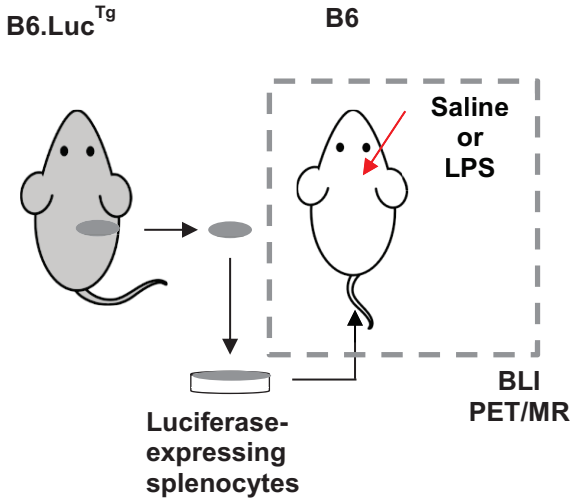

Figure 1-6. Experimental scheme for *in vivo* experiments

Schematic diagram of *in vivo* experimental design using luciferase-expressing splenocytes to visualize peripheral immune cells in the neuroinflammatory mouse model

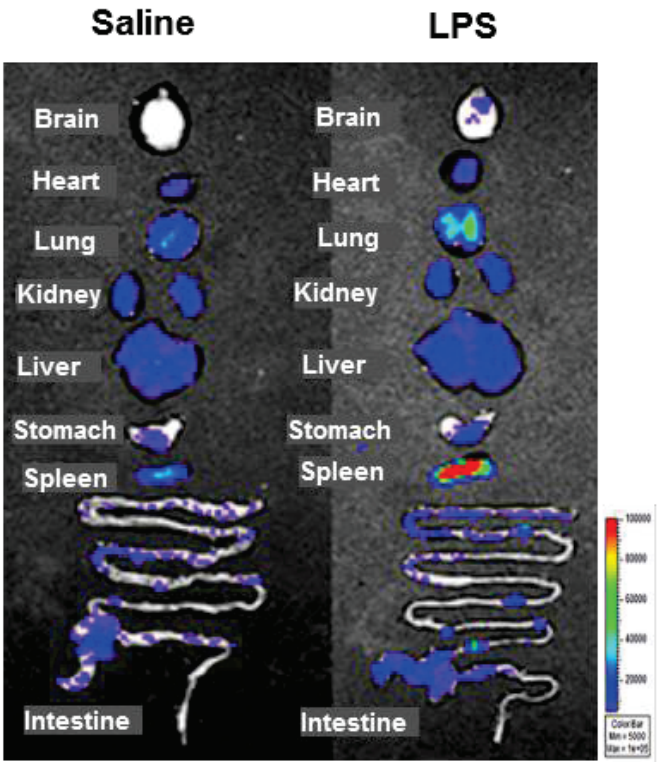

Figure 1-7. Bio-distribution of peripheral immune cells from C57BL/6.Luc^{Tg} The organ distribution of luciferase-expressing splenocytes in intracranial saline or LPS-injected mouse

MRI using Gd-DOTA to monitor the BBB disruption and infiltrated immune cells

I established intracranial mouse models by saline as a control or LPS as an inflammatory model using stereotaxic device with mechanical stress. It was needed to verify injection hole caused by mechanical stress could not induce BBB disruption and inflammatory response for establishing well-controlled experiments. MRI with gadolinium-DOTA (Gd-DOTA, Dotarem®), which is a macrocycle structured-gadolinium based MRI contrast agent, is widely used for imaging of blood vessels and inflamed and disease tissues where abnormalities in BBB occur. Enhanced T1-weighted MR signal of Gd-DOTA was produced by leakage of Gd-DOTA through a damaged BBB into extracellular fluids. On the other hand, T2-weighted MR signal provide information on water or vasogenic edema due to an inflamed immune cells.

Our results showed that T1-weighted MR signal using Gd-DOTA was higher in the right striatum of the LPS-injected mouse than in the saline-injected mouse (control). The MR images demonstrated that BBB disruption by mechanical stress was recovered on day 1, whereas the signal peak of LPS-

induced BBB disruption was observed on day 3. It was also observed that T2 signal was more sensitive than the T1 signal in the LPS-injected mouse (Figure 1-8). In previous study, T2-weighted signal enhancement was generated by trapped gadolinium-based chelates by live immune cells (25). Therefore, high T2 signal in this study was expected that live immune cells were infiltrated in that region.

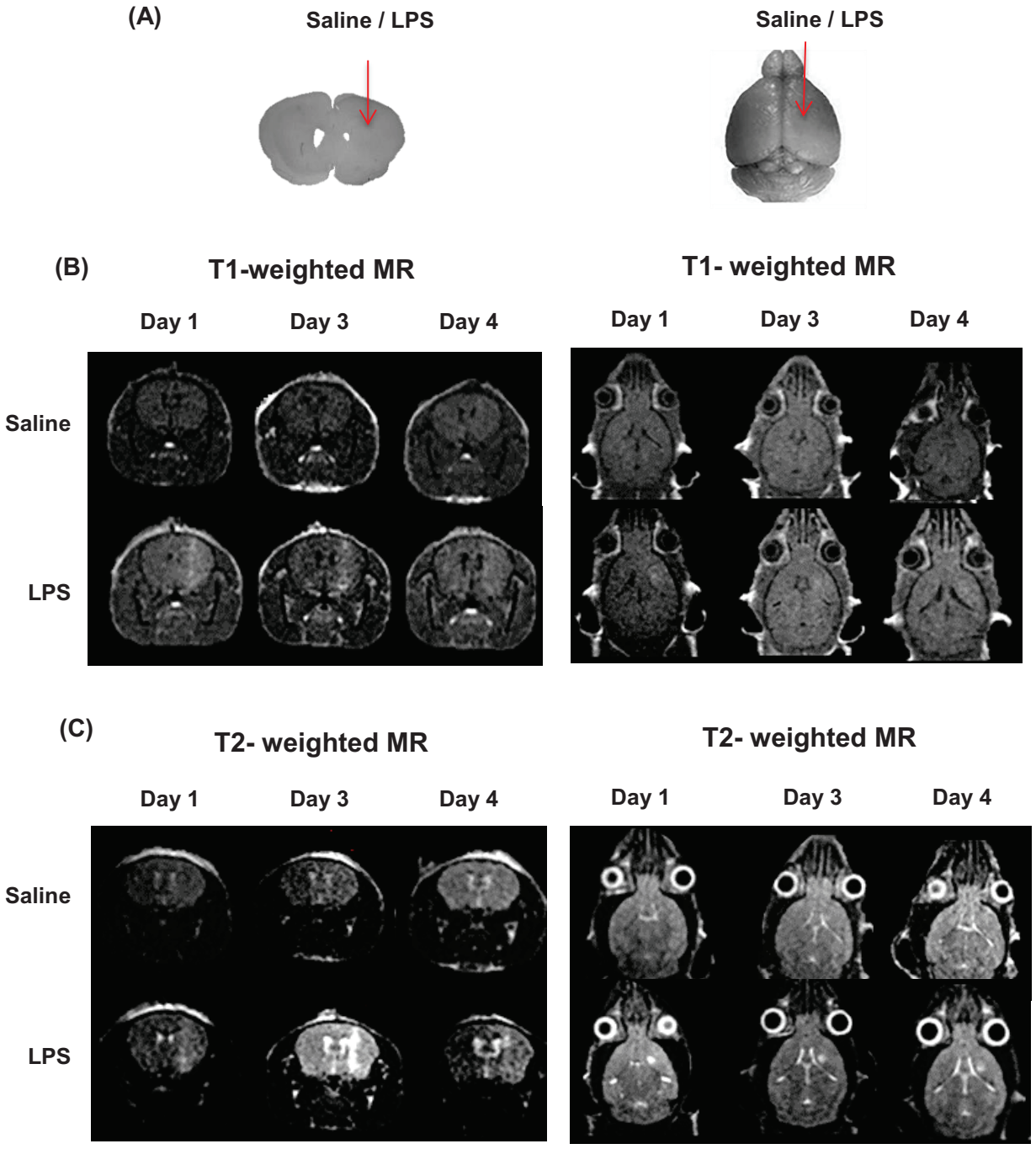
(A)
Saline / LPS
Saline / LPS
(B)
T1-weighted MR
T1- weighted MR
Day 1
Day 3
Day 4
Day 1
Day 3
Day 4
Saline
LPS
(C)
T2- weighted MR
T2- weighted MR
Day 1
Day 3
Day 4
Day 1
Day 3
Day 4
Saline
LPS

Figure 1-8. MR scans using Gadolinium-DOTA for monitoring disruption of Blood-Brain Barrier and infiltrated immune cells

(A) LPS-induced BBB disruption by intracranial injection; saline was used as a control (B) T1-weighted MR scans acquired on days 1, 3, and 4 after intracranial injection (C) T2-weighted MR scans acquired on days 1, 3, and 4 after intracranial injection

Visualization of neuroinflammation using [^{18}F]CB251 PET/MRI and BLI

As I observed the potential that activated immune cells can be distinguished from non-activated immune cells by uptake of [^{18}F]CB251 *in vitro* (Figure 1-4), I expected that [^{18}F]CB251 signals can reflect activated residential immune cells-microglia and peripheral immune cells in the mouse brain.

MR signals showed that the inflammatory response was maintained until 4 days after intracranial LPS injection (Figure 1-8). Thus, to rule out the effects of severe BBB disruption and neuronal tissue damage, [^{18}F]CB251 PET/MRI was acquired 4 days after intracranial injection.

In simultaneous [^{18}F]CB251 PET/MRI, higher [^{18}F]CB251 PET radio-activity was observed in right striatum of intracranial LPS-injected mouse compared to that of control mouse. T2-weighted MR signals in the right striatum of the LPS-induced inflammatory region were also slightly increased. It was found that the critical region of T2-weighted MR signals was co-localized with the region of increased [^{18}F]CB251 PET signals. Bioluminescence images which represent peripheral immune cells infiltration also showed higher optical signals in the right

striatum of the intracranial LPS-injected mouse.

To compare the differences in the strengths of radio-activity and optical signals, the relative level of [^{18}F]CB251 radio-activity and BLI signals in the right and the left striatum of individual brains were acquired. In the saline-injected brain, 1.16-fold higher radio-activity was observed in the right striatum compared to the left striatum (n=6, p=0.012). In the LPS-injected brain, about 1.48-fold higher radio-activity was detected in the right striatum (n=7). For BLI signals, in the control mouse, 1.12-fold higher signal was observed in the right striatum compared to the left striatum, but not significant (n=7). In LPS-injected mouse, 3.45-fold higher signal was exhibited in the right striatum (n=7). These results indicated [^{18}F]CB251 PET was more sensitive to mechanical stress than BLI. I could assume the reason for our results is that [^{18}F]CB251 radioactivity reflect total TSPO activity including activated microglia-brain residential immune cells and infiltrated peripheral immune cells, and BLI signals reflect only injected infiltrated peripheral immune cells. Therefore, the comparative analysis between [^{18}F]CB251 radioactivity and BLI signals was able to provide useful information that reflects the extents of

resident and infiltrated peripheral immune cells activation that occur during neuroinflammation.

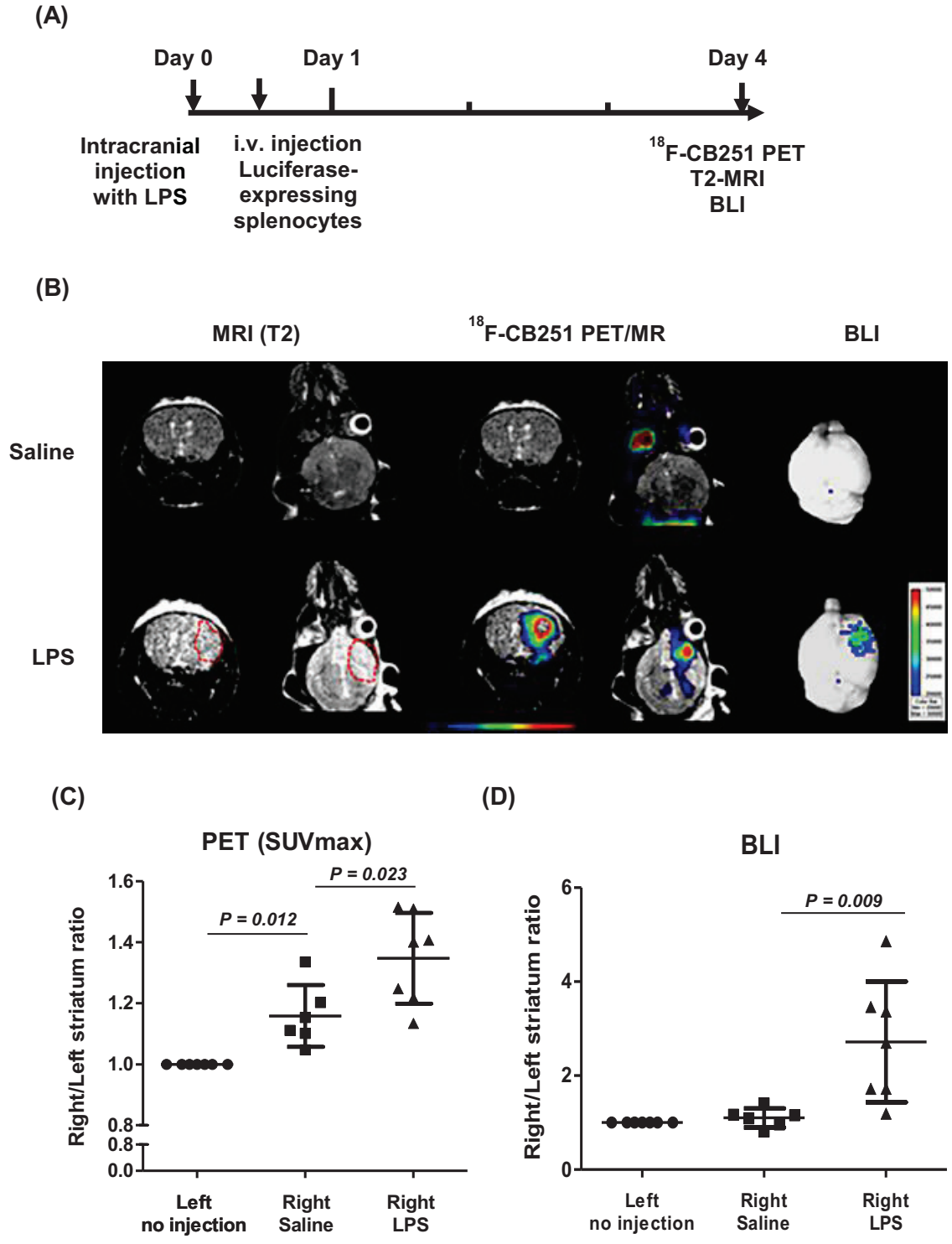
(A)
Day 0
Day 1
Day 4
Intracranial injection with LPS
i.v. injection Luciferase-expressing splenocytes
18F-CB251 PET
T2-MRI
BLI
(B)
MRI (T2)
18F-CB251 PET/MR
BLI
Saline
LPS
(C)
PET (SUVmax)
Right/Left striatum ratio
P = 0.012
P = 0.023
1.6
1.4
1.2
1.0
0.8
0.8
0.0
Left no injection
Right Saline
Right LPS
(D)
BLI
Right/Left striatum ratio
P = 0.009
6
4
2
0
Left no injection
Right Saline
Right LPS

Figure 1-9. [^{18}F]CB251 PET/MRI and BLI in intracranial LPS mouse model (A) Experimental scheme for imaging LPS-induced neuroinflammation with peripheral immune cell infiltration in mice (B) Simultaneous PET/MR images of luciferase-expressing immune cells acquired using [^{18}F]CB251 and BLI (C) Standard uptake value (SUV) max shown as the ratio of the right striatum (saline-injected region, n=6 or LPS-injected region, n=7) to the left striatum in the brain (untreated control) (D) Bioluminescence signal ratio of the right striatum (saline-injected region, n=6 or LPS-injected region, n=7) to the left striatum (untreated control) in the brain

Identification of infiltrated immune cells in neuro-inflammatory region

To identify the types of immune cells in the inflammatory region of the brain, immuno-histochemical staining was performed. TSPO and Luciferase expressing cells (anti-TSPO, anti-luciferase), monocytes (anti-CD68), macrophages (anti-F4/80), microglia (anti-Iba-1) and antigen presenting cells (anti-CD86) showed positive staining in the right striatum of the neuro-inflammatory mouse model. Cytotoxic T cells (anti-CD8) and helper T cells (anti-CD4) were only slightly stained in the same region (Figure 1-10). It was observed that TSPO-expressing cells were co-localized with cells from monocyte lineages, including macrophage and microglia, in the inflammatory area. In addition, antigen presenting cells that express CD86 which is only expressed in peripheral immune cells were positive stained in the right striatum. In general, the ability of antigen presenting is known to be higher in macrophage or dendritic cells of peripheral immune cells than in microglia cells, which play a critical role in T cell activation and deepen inflammation. In this study, the brain tissue was acquired 4 days after intracranial LPS injection for IHC, which was not enough to confirm T cell

activation. However, our results indicated that microglia and infiltrated peripheral immune cells expressing TSPO are present at the site of inflammation, which was consistent with the results of our multi-modal imaging.

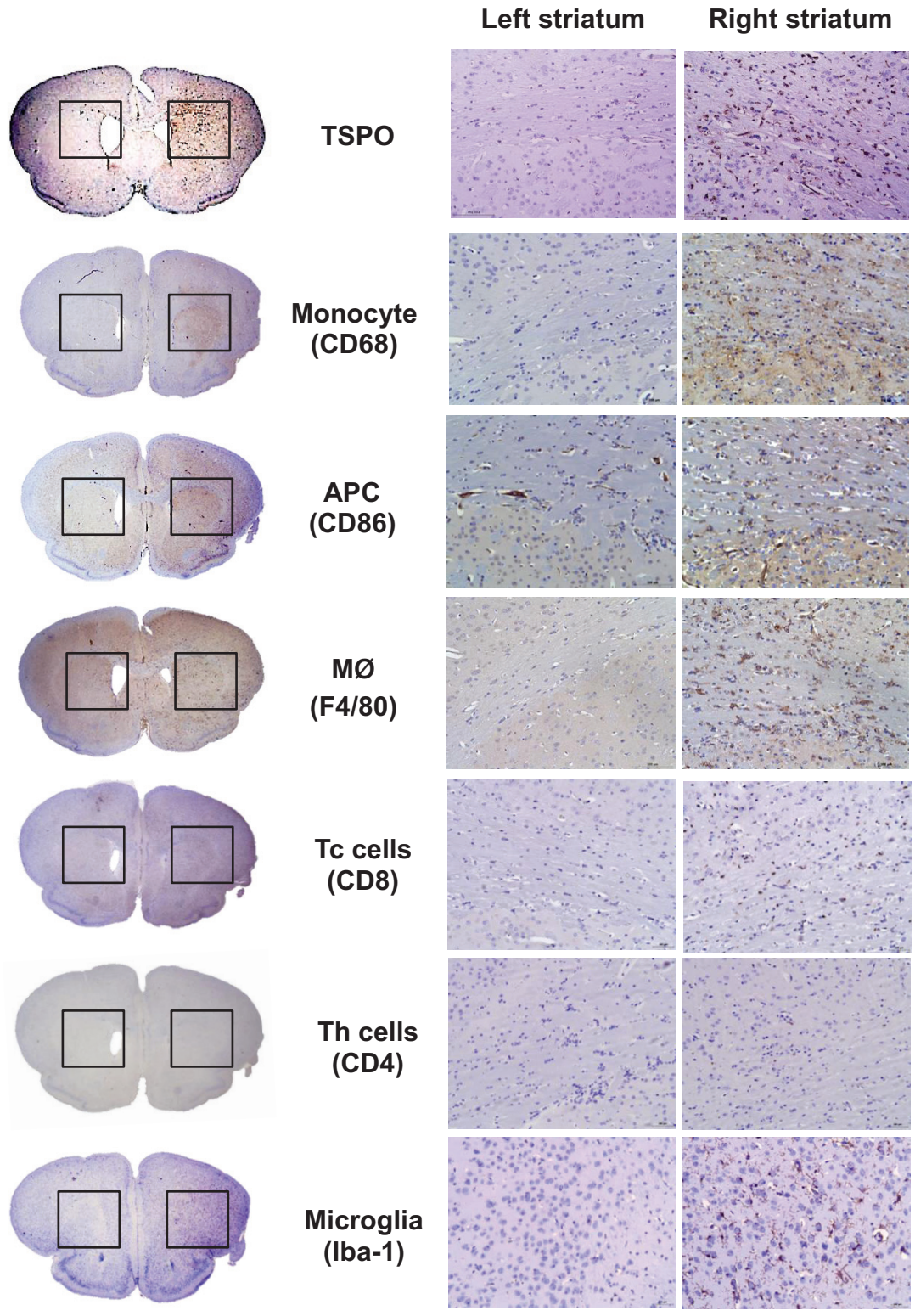
Left striatum
Right striatum
TSPO
Monocyte
(CD68)
APC
(CD86)
MØ
(F4/80)
Tc cells
(CD8)
Th cells
(CD4)
Microglia
(Iba-1)

Figure 1-10. Immuno-histochemical staining of the brain tissue of intracranial LPS mouse model TSPO-expressing cells (anti-TSPO), Monocytes (anti-CD68), antigen-presenting cells (anti-CD86), macrophages (anti-F4/80), cytotoxic T cells (anti-CD8), helper T cells (anti-CD4), and microglia and macrophages (anti-Iba-1) were stained.

Comparative analysis of neuro-inflammation by [^{18}F]CB251 PET/MRI and BLI after treatment of anti-inflammatory agent, CDDO-Me

I next investigated whether anti-inflammatory impact of agents could be evaluated using our multi-modal imaging including [^{18}F]CB251 PET/MRI and BLI. Anti-inflammatory agent, CDDO-Me, which is known to inhibit inflammatory cytokines (26, 27), was treated into mouse model once a day for total of three injections (Figure 1-11, 1-12A, 200 nM/mice). The efficacy of anti-inflammatory agent was identified and compared by two ways: PET/MRI scan using [^{18}F]CB251 and BLI signal representing splenocytes. [^{18}F]CB251 uptake ratio (SUVmax, right/left striatum) showed 1.39-fold (n=12) higher uptake in LPS injected mouse (p=0.002), 1.23-fold (n=5) higher uptake in LPS and CDDO-Me treated mouse (p=0.0323) compared to saline-injected mouse (n=8). The similar pattern was also confirmed in the ratio of SUV mean value. In addition, BLI ratio of total photon flux (right/left striatum) in LPS-injected mouse were 3.85-fold (p=0.0009, n=12) higher and those in LPS and CDDO-Me treated mouse were 1.90-fold (p=0.0025, n=5) higher than that of saline-injected mouse (n=8) after skin

removal (Figure 1-12). [^{18}F]CB251 PET signals revealed that the inflammatory response was attenuated by CDDO-Me treatment. BLI signals showed that CDDO-Me inhibited recruitment of peripheral immune cells at the site of inflammation. These data demonstrate that [^{18}F]CB251 PET is useful non-invasive imaging for assessing therapeutic efficacy of total inflammatory response. According to these results, there is more significant difference in the BLI signals of extracted brain tissue.

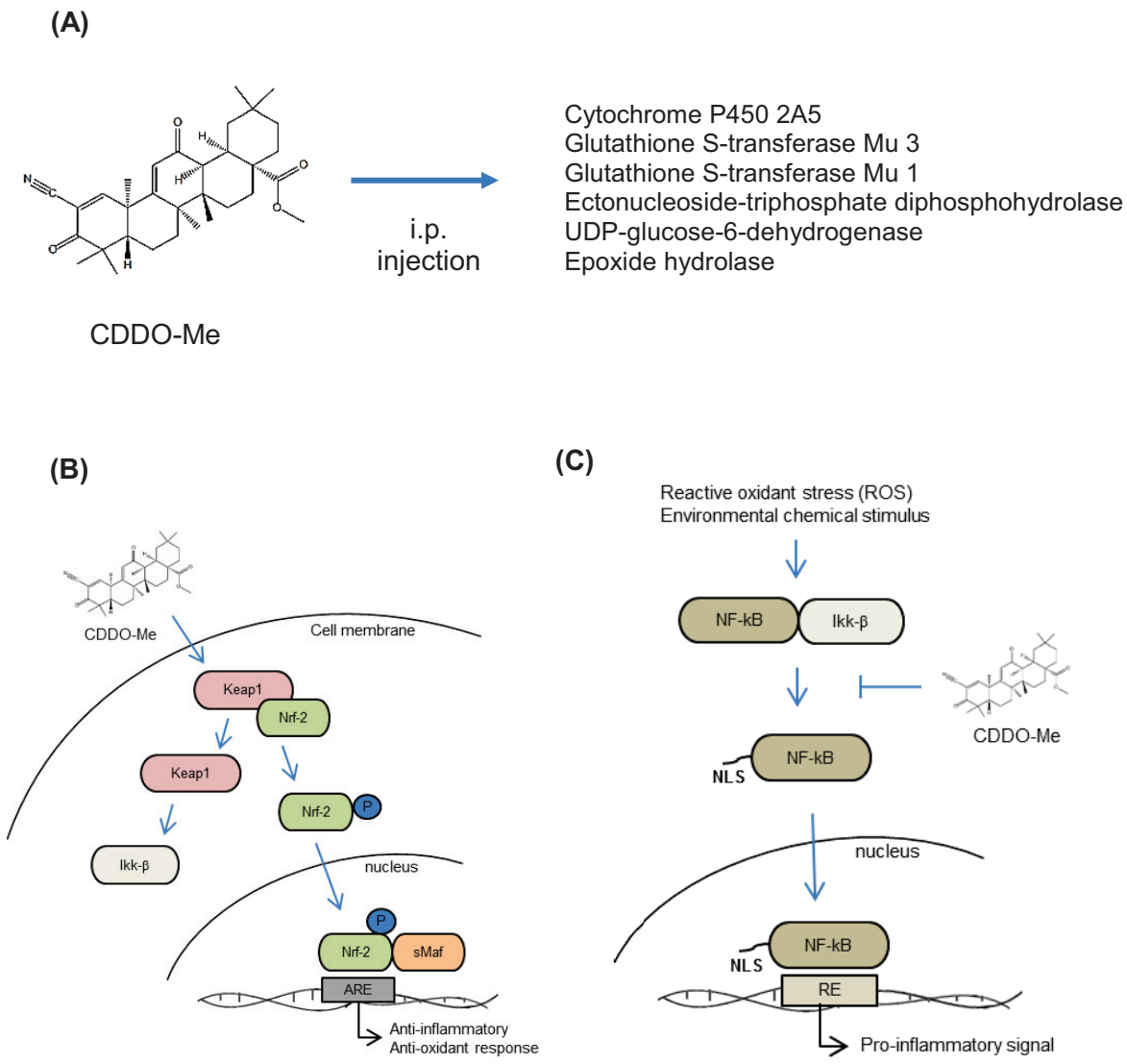

Figure 1-11. The functional mechanisms of CDDO-Me (A) Upregulated genes by intraperitoneal injection of CDDO-Me (B) The mechanism of CDDO-Me in anti-inflammatory response (C) Inhibitory mechanism of CDDO-Me in pro-inflammatory response

(A)

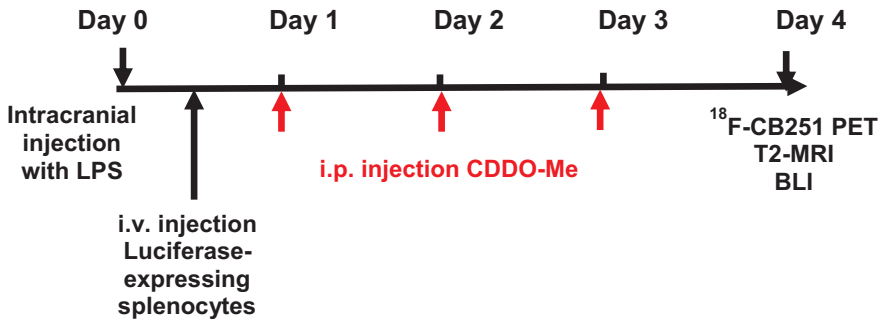
Day 0
Day 1
Day 2
Day 3
Day 4
Intracranial injection with LPS
i.v. injection Luciferase-expressing splenocytes
i.p. injection CDDO-Me
18F-CB251 PET
T2-MRI
BLI

(B)

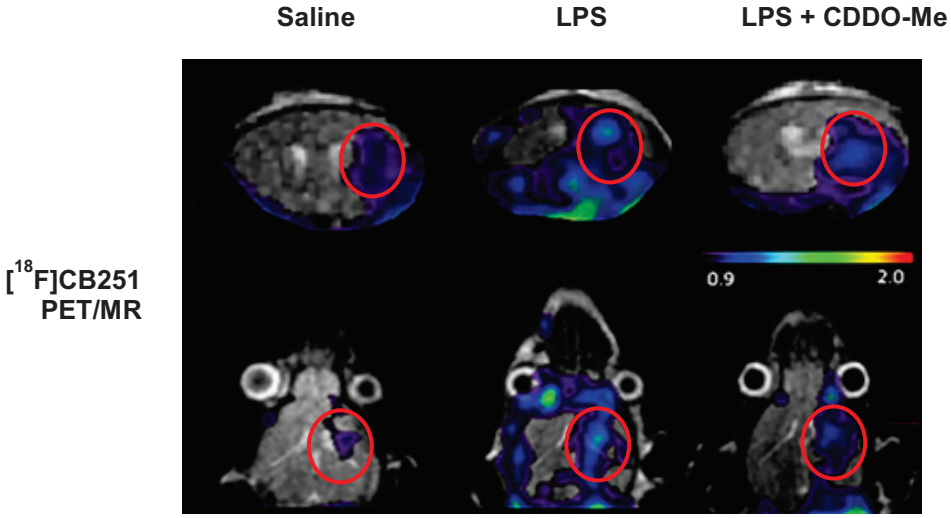
Saline
LPS
LPS + CDDO-Me
[18F]CB251 PET/MR
0.9
2.0

(C)

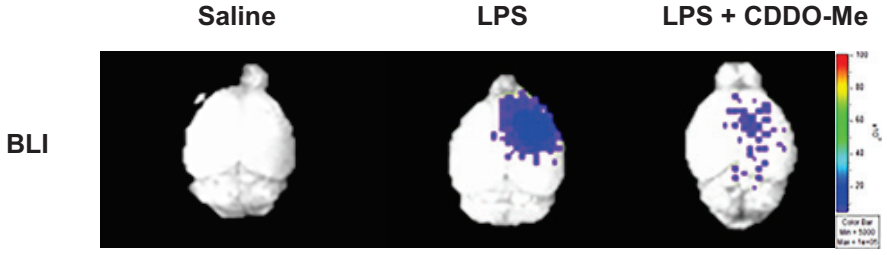
Saline
LPS
LPS + CDDO-Me
BLI

(D)

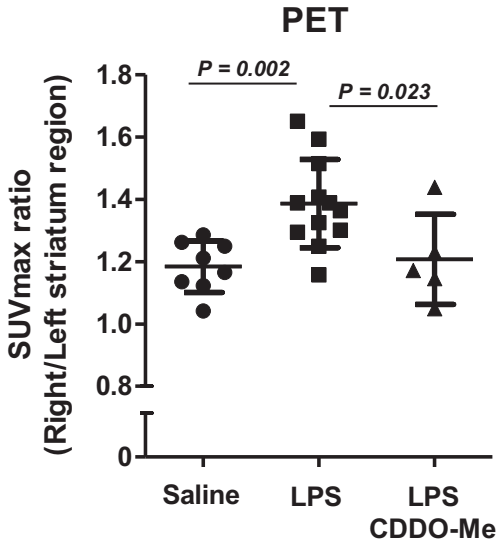
PET
P = 0.002
P = 0.023
SUVmax ratio
(Right/Left striatum region)
1.8
1.6
1.4
1.2
1.0
0.8
0
Saline
LPS
LPS
CDDO-Me

(E)

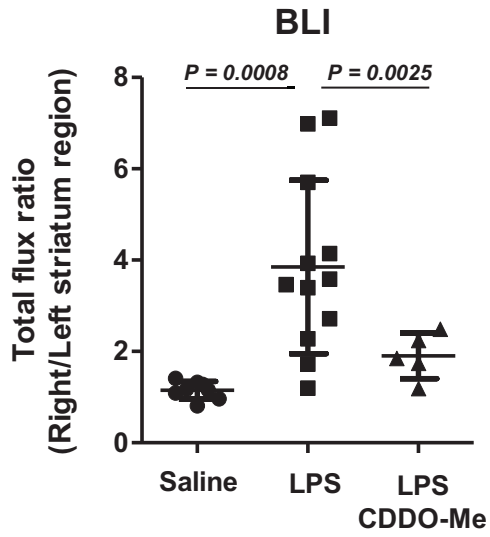
BLI
P = 0.0008
P = 0.0025
Total flux ratio
(Right/Left striatum region)
8
6
4
2
0
Saline
LPS
LPS
CDDO-Me

Figure 1-12. Evaluation of the therapeutic effect of anti-inflammatory agent using [^{18}F]CB251 PET/MRI and BLI

(A) Experimental scheme for treatment of anti-inflammatory agent (B) Representative images of simultaneous PET/MR scans acquired in saline-injected, LPS-injected, or LPS- and CDDO-Me-treated mouse model (C) Representative bioluminescent images acquired in saline-injected, LPS-injected, or LPS- and CDDO-Me-treated mouse model (D) The standard uptake value (SUV) max ratio of [^{18}F]CB251 PET in the control (n=8), LPS-injected (n=12), LPS and CDDO-Me-treated (n=5) mouse model (E) The ratio of total photon flux (right/left striatum) in the control (n=8), LPS-injected (n=12), LPS and CDDO-Me-treated (n=5) mouse model

DISCUSSION

In chapter 1, I confirmed [^{18}F]CB251 was bound to the TSPO protein *in vitro* and *in vivo* indicating [^{18}F]CB251 as a promising PET probe for targeting neuroinflammation. [^{18}F]CB251 radio-activity included the effect of microglia-residential immune cells and infiltrated peripheral immune cells. MR scans showed BBB disruption caused by LPS, and BLI signals represented infiltrated peripheral immune cells in the inflammatory region. Therefore, I successfully visualized immune cell recruitment in the inflammatory region of the brain using [^{18}F]CB251 PET and demonstrated [^{18}F]CB251 PET signal could reflect the severity of neuroinflammation in acute neuroinflammatory models.

I investigated specific binding between the [^{18}F]CB251 ligand and TSPO protein *in vitro* and applied it *in vivo.* By regulating TSPO expression, [^{18}F]CB251 uptake was specific to TSPO (Figure 1-3, 4). However, changes in [^{18}F]CB251 uptake were not directly proportional to the degree of TSPO expression indicating further studies would be needed to explore other mechanisms related to [^{18}F]CB251 uptake.

In our previous study, I confirmed functions of luciferase-

expressing immune cells from reporter transgenic mouse were not different from those of immune cells of a normal mouse (28). The immune cell composition and cellular immunity after syngeneic or allogenic transfer in luciferase-expressing transgenic mouse (B6.Luc^{Tg}) were similar to those of normal mouse (C57BL/6 or B6) (Figure 1-5, table 2). These results indicated luciferase-expressing splenocytes were able to reflect the normal immune response. I found that the intravenous administration of luciferase-expressing splenocytes showed different distribution patterns in the brain depending on various mouse models i.e., saline, LPS, and LPS treated with CDDO-Me groups (Figure 1-12). These results demonstrated that the number of infiltrated splenocytes reflected the degree of inflammation.

I visualized BBB disruption by LPS injection using MRI with gadolinium-DOTA (Gd-DOTA, Dotarem®), which is a macrocycle structured-gadolinium based MRI contrast agent (Figure 1-8). It is widely used for imaging of blood vessels and inflamed and disease tissues where abnormalities in blood brain barrier occur. The paramagnetic property of Gd-DOTA reduces

T1-relaxation time produced by leakage of Gd-DOTA through a damaged BBB into extracellular fluids and induces contrast enhancement (29, 30). According to recent study (25), T1 contrast enhancement was due to fast diffusing of gadolinium based chelates present outside of cells by dead cells and T2 contrast enhancement represented slow diffusing of gadolinium based chelates present in live immune cells. Thus, it was expected our MR data indicated BBB disruption and infiltrated live immune cells in the neuro-inflammatory model. MR images using Gd-DOTA showed no significant enhancement in the brain of the saline-injected mouse and mechanical disruption was recovered at day 1 after saline injection (Figure 1-8).

To verify the multi-modal imaging could be used for evaluating the therapeutic efficacy, an anti-inflammatory drug, CDDO-Me, was used in our inflammatory mouse model. CDDO-Me is known as an agonist of the KEAP1-Nrf2 pathway targeting the pro-inflammatory transcription factor, NF-kB (26, 31-34), which induces the expression of antioxidant proteins and thus protects against oxidative damage from injury and inflammation (Figure 1-11). In the LPS-treated inflammatory mouse model,

treatment with CDDO-Me decreased [^{18}F]CB251 PET and BLI signals indicating reduced inflammatory response and decreased recruitment of peripheral immune cells (Figure 1-12). BLI signal showed a larger change than PET signal. Thus, CDDO-Me appeared to influence the infiltration of peripheral immune cells suggesting [^{18}F]CB251 uptake reflected the effects of both infiltrating peripheral immune cells and the resident microglia. Immunohistochemical staining confirmed the presence of inflammatory monocytes, macrophages, antigen presenting cells, and cytotoxic T cells in inflammatory regions together with resident immune cells, microglia (Figure 1-10). Further studies are needed to investigate an interaction between residential immune cells and peripheral immune cells in the pathogenesis of neuroinflammation.

Several studies show that prolonged neuroinflammation is linked to the onset and the progression of neurodegeneration. Neurodegeneration is a condition which is characterized by the loss of the neuronal structure and functions so it can cause several diseases such as Alzheimer' s disease, Parkinson' s disease and Multiple sclerosis (2, 35). Causative mechanisms of

neurodegeneration are still unclear. However, several pathways related to neuroinflammation have roles in process of neurodegenerative disease (2, 36, 37). For example, systemic and local CNS inflammation has been identified to be associated with cerebral small vessel disease (SVD)–vascular dementia. Chronic hypoperfusion due to inflammation induces oligodendrocyte death and the continuous degeneration of myelinated fibers that amplify the risk of stroke (38). Also, vascular inflammation according to infiltration of monocytes into the injured and loosened vascular wall acts as a major risk factors of CNS tissue disruption (39). Therefore, I expect development of [^{18}F]CB251 PET imaging for neuroinflammation could be useful technique for predicting neurodegenerative diseases.

In chapter 1, I showed distinct effects of brain residential immune cells and peripheral immune cells on neuroinflammation. Also, the action of an anti-inflammatory drug on CNS and peripheral immunity could be confirmed with our imaging strategy. I believe that our multi-modal imaging approach can help better understand the interaction between CNS immunity and peripheral

immunity in neuro-pathogenesis. Furthermore, the efficacy of several anti-inflammatory medications could be investigated, and a treatment plan could be established using our multi-modal imaging.

Conclusion

I established multi-modal imaging using three different methods (BLI, [^{18}F]CB251 PET, MRI) for investigating neuro-inflammation in acute neuroinflammatory model. Our strategy was to visualize neuroinflammation by identifying recruited peripheral as well as resident immune cells in neuroinflammatory region. I demonstrated the potential of [^{18}F]CB251 as a promising radiotracer for the diagnosis of neuroinflammation. The therapeutic effect of an anti-inflammatory drug in LPS-induced neuro-inflammation could also be monitored. Our findings suggest that multi modal imaging using PET/MR/BLI is a useful technique for basic and clinical studies related to neuroinflammation.

CHAPTER 2

Evaluation of [^{18}F]CB251 as a polymorphism independent TSPO-targeting PET tracer

INTRODUCTION

2.1 TSPO-targeting radiotracers and [^{18}F]CB251

To date, [^{11}C]PK11195 and [^{11}C]PBR28 have been mainly used as TSPO-targeting probes. However, several TSPO PET probes still have limitations such as non-specific binding and a low target-to-background ratio (13, 40, 41). [^{11}C]PBR28 was also reported that responder states have been divided into high-, mixed-, and low-affinity binders according to TSPO polymorphism (42). In addition, carbon-11 [^{11}C] labeled ligand shows time limitation due to short half-life, 20.3 min. Therefore, fluorine-18 [^{18}F] TSPO radiotracers, which have a longer half-life (109.8 min), have been developed. Currently, our group developed [^{18}F]CB251 ligand as a promising TSPO radiotracer. This ligand showed higher TSPO affinity and longer half-life than [^{11}C]PK11195 (20, 43). Therefore, I applied [^{18}F]CB251 as a novel PET probe for the imaging of inflammatory cells in neuroinflammatory region in Chapter 1. In Chapter 2, I evaluated that CB251 does not affect binding affinity by polymorphism, a major limitation of 2nd generation TSPO ligands.

2.2 TSPO polymorphism, a major limitation of 2nd generation TSPO ligands

PK11195 as a 1st generation TSPO ligand showed low binding affinity to TSPO and high off-target effect in human studies (44, 45). Therefore, 2nd generation TSPO ligands including PBR28 were developed, which showed promising properties in both *in vitro* and *in vivo* studies. But, in early human PET studies, PBR28 displayed the greater inter-variability by TSPO rs6971 polymorphism (46). TSPO gene is located chromosome 22q13.31; 4 exons and has a variety of single nucleotide polymorphisms (SNPs). In specific, most frequently observed non-synonymous SNP, TSPO Ala147Thr mutant (Figure 2-1A, B), which is present in about 30% of the Caucasian was main cause of lower TSPO binding affinity of [^{11}C]PBR28. In order to evaluate the clinical application of the new TSPO ligand, it is important to compare the binding affinity of ligand according to TSPO genetic variants.

2.3 The aim of the study

In chapter 2, I compared the binding affinity of CB251 ligand to TSPO WT and TSPO A/T Mut (rs6971). Vector system for WT

and A/T Mut was established and conducted cell uptake, phantom study with 293FT cells expressing TSPO WT or A/T Mut. In addition, competitive inhibition assay was performed for measuring IC_{50} of each genetic variant using CB251 and [^{3}H]PK11195. I confirmed that CB251 ligand exhibited similar binding affinity on WT and A/T Mut. These results indicated that [^{18}F]CB251 is a promising polymorphism independent TSPO-targeted radiotracer.

Table 3. Comparison of TSPO-targeting ligands in terms of rs6971 polymorphism

TSPO ligand	K_i (nM) of TSPO WT	K_i LAB/HAB	IC_{50} LAB/HAB	Radioisotope	Clinical study	Limitations on radiotracer
PK11195	26[a, c]	0.85[a]	0.86	Carbon-11	Neuropathology, Glioma	Low TSPO binding affinity, High off-target effect, Low signal-to-background ratio
PBR28	3.4[a]	55[a]	-	Carbon-11	Autism spectrum disorder, Neurodegenerative diseases	High inter-individual variability by polymorphism
Fm-PBR28-*d2*	3.6[b]	-	37.28	Fluorine-18	-	High inter-individual variability by polymorphism
DPA-713	4.7[a, d]	4.4[a]	-	Carbon-11	TSPO PET tracer in brain	High inter-individual variability by polymorphism
XBD-173	0.29[a]	15[a]	-	Carbon-11	Neuroinflammation, Anxiety, Panic disorder, Depression	High inter-individual variability by polymorphism, Used drug
CB251	0.27[a]	-	1.14	Fluorine-18	-	High TSPO binding affinity

Ref. a)50, b)49, c)44, d)51

MATERIALS AND METHODS

1. Cell culture

To establish cells with TSPO genetic variants, 293FT cells were maintained in complete DMEM (10% FBS and 1% antibiotics) with L-Glutamate (2 mM), Sodium pyruvate (1 mM) and MEM NEAA.

2. Transient transfection for TSPO WT and A147T Mutant expression

To express the polymorphic TSPO proteins (Wile type;WT, Mutant with Ala → Thr at 147 amino acid; A147T), Different TSPO gene with site mutagenesis from the PBR(TSPO) (NM_000714) human tagged ORF clone RG220107 (Origene, Rockville, MD, USA) were generated. I changed the 147 amino acid Alanine to Threonine (A147T) by changing the nucleotide sequences from Guanine to Adenine. These vectors were transfected into 293FT cells for 24 hours and conducted in vitro uptake.

3. Membrane protein isolation

Membrane protein was extracted by protocols from membrane

protein extraction kit (Mem-PER plus kit, Thermo fisher). 293FT cells (5 x 10^6/100 Ø) were plated for transient transfection. 293FT cells were transiently transfected with TSPO WT or A147T vector for 24 hours. Cells were collected using scraper, washed twice with cell wash solution and centrifuged (300 x *g*, 5 min, 4° C). Cell pellet was permeabilized for 10 min at 4° C. Membrane pellet was harvested after centrifugation (16000 x *g*, 15 min, 4° C) and supernatant containing cytosolic protein was removed. Membrane pellet was resuspended using solubilization buffer in Mem-PER plus kit for 30 min at 4° C with mixing. The tube was centrifuged one more (16000 x *g*, 15 min, 4° C) and then supernatant containing membrane proteins was harvested and used for competitive binding assay.

4. [^{18}F]fm-PBR28-*d2* radiochemistry

All materials and methods and synthesized [^{18}F]fm-PBR28-*d2* were provided by our group in Bundang Seoul national university hospital. The [^{18}F]fluoromethyl-PBR28 substituted with deuterium ([^{18}F]fm-PBR28-d_2) was synthesized according to a previous study[48]. [^{18}F]Fluoride was produced by the ^{18}O (p,n)^{18}F

nuclear reaction using $H_2{}^{18}O$ as the target material was loaded onto a chromafix-HCO_3 cartridge to remove the enriched water, then eluted by the mixture of $K_{2.2.2}/K_2CO_3$ dissolved in a 10% water/methanol solution. Azeotropic distillation of the eluted solution was performed with 1 mL of acetonitrile under nitrogen stream (×2). Dibromomethane-d_2 (50 μL) in acetonitrile was incubated with the dried complex of $K^{18}F$ /$K_{2.2.2}$. The mixture was heated at 120°C for 5 min, then passed through a Sep-Pak cartridge with C18 to remove remaining precursors and trapped the bromo[^{18}F]fluoromethane-d_2 in 0.7 mL of *N,N*-dimethylformamide under ice bath. This mixture was then transferred to a reaction vial containing 1 mg of desmethyl-PBR28 and 6 μL of 5 N NaOH. The reaction mixture was heated at 100 °C for 5 min, cooled to 25 °C and diluted with 10 mL of distilled water. This solution was passed through a C18 plus Sep-Pak cartridge, washed with water (10 mL), and eluted with CH_3CN (1.5 mL). The eluted solution was analyzed by a semi-prep HPLC system (Waters, Xterra RP-18 10 × 250 mm, 10μm; 45% acetonitrile/water, flow rate 3 mL/min, λ = 254 nm.) equipped with UV and gamma-ray detectors. The final product of [^{18}F]fm-PBR28-*d2* was collected after 13.5 min,

diluted by 20 mL of water, loaded onto a C18 plus Sep-Pak cartridge, and then eluted by an 8% ethanol/saline solution to remove HPLC solvent.

5. *in vitro* uptake with [^{11}C]PK11195, [^{18}F]CB251 and [^{18}F]fm-PBR28-d_2

All procedures were performed in the same way as in Chapter 1. The cells were preincubated with glucose-free RPMI1640 medium (Gibco) for 4 hours before *in vitro* uptake. Cells were trypsinized, counted and transferred to 5 mL test tube. 1×10^5 cells were suspended in the pre-warmed Hank's balanced salt solution (HBSS, Sigma-Aldrich) containing 0.5% (w/v) bovine serum albumin (BSA, Sigma-Aldrich). 0.185 MBq of [^{11}C]PK11195, [^{18}F]CB251 or [^{18}F]fm-PBR28-d_2 were added to the tubes, and the cells were maintained in a humidified 37° C incubator with 5% CO_2 for 1 hour. The cells were washed three times with cold HBSS and radioactivity was measured by a Cobra II gamma counter (Canberra Packard). The cells were then lysed for 5 min using 1% sodium dodecyl sulfate solution (total volume 200 μL, SDS, Sigma-Aldrich). Cell lysates were collected and total protein concentrations were analyzed by the BCA assay kit

(Pierce). Radioactivity was normalized according to the amount of total protein at the time of assay. All experiments were performed in triplicate.

6. Competitive inhibition assay

To compare binding affinity of TSPO-targeting ligands according to TSPO polymorphism, competitive inhibition assay using [^{3}H]PK11195 radiotracer and 3 different TSPO-targeting ligands, fluoromethyl-PBR28-*d2*, CB251, PK11195 was conducted. Membrane protein (100 μg/100 μL) extracted from 293FT cells expressing TSPO WT or TSPO A147T mutant protein was mixed with [^{3}H]PK11195 (0.019 MBq/100 μL) and 9 concentrations of each ligand (from 0.1 nM to 1000 μM) in assay buffer (50 mM Tris base, 140 mM NaCl, 1.5 mM $MgCl_2$, 5 mM KCl, 1.5 mM $CaCl_2$, pH 7.4) for 1 hour at 37° C. Assay tubes were passed through whatman filter using vacuum system and then the filter containing the membrane protein was washed three times using wash buffer (50 mM Tris base, 1 mM $MgCl_2$, pH7.4) (47). Radioactivity of each filter was measured with β-counter (Liquid scintillation analyzer Tri-Carb3100 TR, Perkin Elmer) with scintillation buffer (Perkin Elmer).

RESULTS

TSPO wildtype and TSPO rs6971

To compare binding affinity of [^{18}F]CB251 according to TSPO Ala147Thr (TSPO A/T Mut), vector systems expressing TSPO wildtype or TSPO A/T mutant gene were established (Figure 2-1).

(A)

Polymorphism (rs6971)	Protein
C/C	Ala/Ala (HAB)
C/T	Ala/Thr (MAB)
T/T	Thr/Thr (LAB)

(B)

TSPO gene wildtype ORF sequence

ATGGCCCCGCCCTGGGTGCCCGCCATGGGCTTCACGCTGGCGCCCAGCCTGGGGTGC
TTCGTGGGCTCCCGCTTTGTCCACGGCGAGGGTCTCCGCTGGTACGCCGGCCTGCAG
AAGCCCTCGTGGCACCCGCCCCACTGGGTGCTGGGCCCTGTCTGGGGCACGCTCTAC
TCAGCCATGGGGTACGGCTCCTACCTGGTCTGGAAAGAGCTGGGAGGCTTCACAGAGA
AGGCTGTGGTTCCCCTGGGCCTCTACACTGGGCAGCTGGCCCTGAACTGGGCATGGC
CCCCCATCTTCTTTGGTGCCCGACAAATGGGCTGGGCCTTGGTGGATCTCCTGCTGGT
CAGTGGGGCGGCGGCAGCCACTACCGTGGCCTGGTACCAGGTGAGCCCGCTGGCCG
CCCGCCTGCTCTACCCCTACCTGGCCTGGCTGGCCTTCGCGACCACACTCAACTACTG
CGTATGGCGGGACAACCATGGCTGGCATGGGGGACGGCGGCTGCCAGAG

TSPO A147T mutant gene ORF sequence (rs6971)

ATGGCCCCGCCCTGGGTGCCCGCCATGGGCTTCACGCTGGCGCCCAGCCTGGGGTGC
TTCGTGGGCTCCCGCTTTGTCCACGGCGAGGGTCTCCGCTGGTACGCCGGCCTGCAG
AAGCCCTCGTGGCACCCGCCCCACTGGGTGCTGGGCCCTGTCTGGGGCACGCTCTAC
TCAGCCATGGGGTACGGCTCCTACCTGGTCTGGAAAGAGCTGGGAGGCTTCACAGAGA
AGGCTGTGGTTCCCCTGGGCCTCTACACTGGGCAGCTGGCCCTGAACTGGGCATGGC
CCCCCATCTTCTTTGGTGCCCGACAAATGGGCTGGGCCTTGGTGGATCTCCTGCTGGT
CAGTGGGGCGGCGGCAGCCACTACCGTGGCCTGGTACCAGGTGAGCCCGCTGGCCG
CCCGCCTGCTCTACCCCTACCTGGCCTGGCTGGCCTTC**A**CGACCACACTCAACTACTG
CGTATGGCGGGACAACCATGGCTGGCATGGGGGACGGCGGCTGCCAGAG

(C)

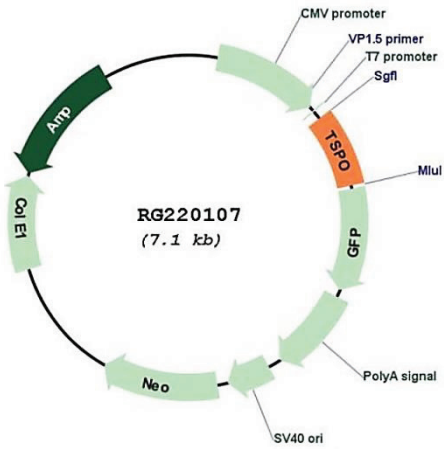

Figure 2-1. Vector system for establishing TSPO wildtype and TSPO rs6971

(A) TSPO genetic variants and amino acid sequence (B) Open reading frame sequence of TSPO wildtype and TSPO Ala147Thr single nucleotide polymorphism (rs6971) (C) Vector construct for expressing TSPO WT and TSPO A/T Mut

Comparison of [^{18}F]fm-PBR28-*d2* and [^{18}F]CB251 uptake according to TSPO polymorphism

The binding affinity of CB251 was higher than the binding affinities of PK11195 and PBR28 which is widely used TSPO ligands (Table 3, Figure 2-2A)(48, 49). [^{18}F]CB251 has improved affinity to TSPO protein. To identify the difference in binding affinity of [^{18}F]CB251 according to TSPO wildtype and TSPO A/T Mut, I constructed two 293FT cell lines which express the most abundant type (wildtype) and mutant type (A/T Mut). And compared with [^{18}F]fm-PBR28-*d2*, which is known to show the difference in binding affinity according to TSPO polymorphism (TSPO A/T Mut). Our cell uptake of [^{18}F]CB251 showed similar cellular uptake levels, regardless of the TSPO polymorphism. On the other hand, cell uptake level of [^{18}F]fm-PBR28-*d2* was decreased by about 72% according to TSPO polymorphism (Figure 2-2B). This indicates [^{18}F]CB251 is suitable and good for use as a TSPO-targeting PET radiotracer.

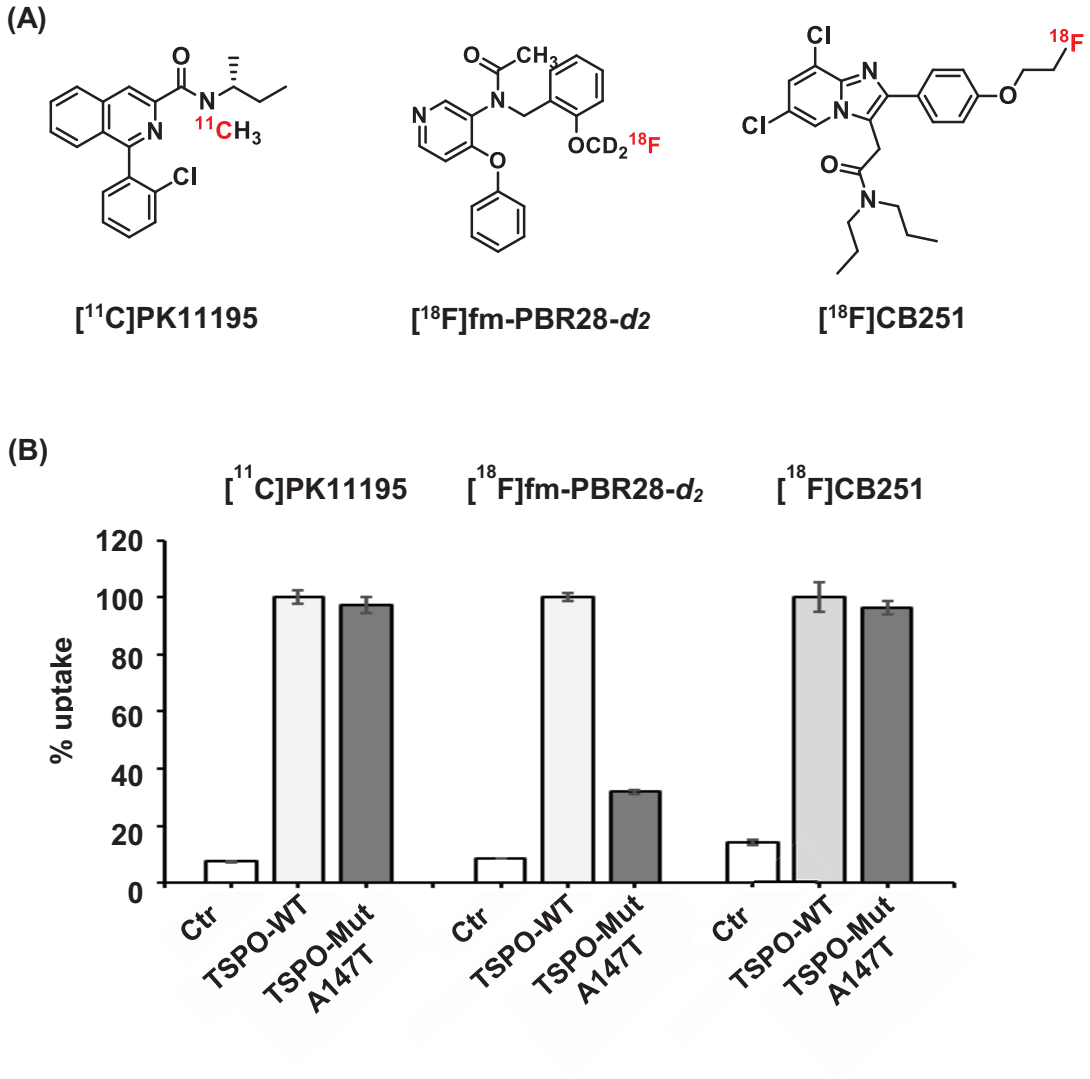

Figure 2-2. *In vitro* cell uptake of TSPO-targeting ligands, [^{18}F]PBR28 and [^{18}F]CB251, according to TSPO polymorphism (A) Structure of CB251 and PK11195, PBR28 compound (16, 43) (B) *in vitro* [^{11}C]PK11195, [^{18}F]PBR28 and [^{18}F]CB251 uptake in 293FT expressing TSPO WT and TSPO A/T Mut (in triplicate)

Evaluation of [^{18}F]fm-PBR28-*d2* and [^{18}F]CB251 uptake by TSPO polymorphism in PET scan

I found no difference in [^{18}F]CB251 uptake between cells expressing TSPO WT and TSPO A/T Mut, unlike [^{18}F]fm-PBR28-*d2* uptake. To determine whether this cellular uptake is reflected in PET imaging, PET scans of each PET probe were obtained from 293FT expressing TSPO WT and TSPO A/T Mut and mice bearing these cells. The ratio of SUVmax (TSPO WT/ TSPO A/T Mut) was found to be about 5.43-fold in cells and 4.11-fold in mice for [^{18}F]fm-PBR28-*d2*. In the case of [^{18}F]CB251, the ratio of SUVmax (TSPO WT/ TSPO A/T Mut) was about 1.67-fold in cells and 1.38-fold in mice (Figure 2-3). These results, in parallel with the results of in vitro uptake, indicate that differences in ligand uptake with TSPO polymorphism were also identified in PET scans.

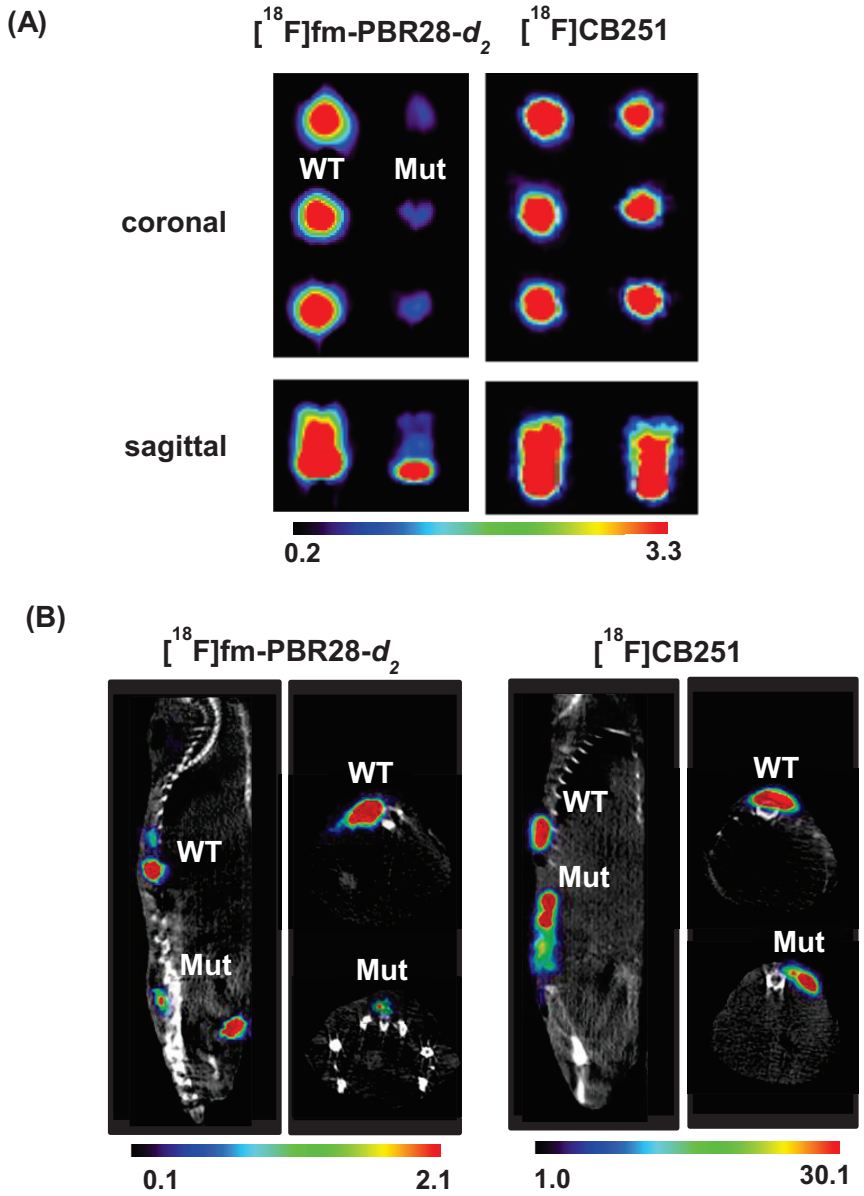

Figure 2-3. PET/CT imaging of TSPO-targeting ligands in 293FT expressing TSPO WT or TSPO A/T Mut

(A) PET scan of [^{18}F]fm-PBR28-*d2* and [^{18}F]CB251 in 293FT expressing TSPO WT or A/T Mut (n=3) (B) PET/CT images of mice bearing 293FT expressing TSPO WT or A/T Mut (n=2)

Comparison of inhibitory concentration (IC_{50}) according to TSPO ligand

To validate that the differences of cellular uptake according to each PET probe are due to TSPO-specific binding, I conducted competitive inhibition assay in membrane proteins isolated from 293FT expressing TSPO WT and TSPO A/T Mut. I identified and established appropriate concentration of membrane proteins for competitive inhibition assay using [^{18}F]PBR28 with different binding affinity in TSPO A/T Mut. The uptake increased with the concentration of membrane proteins isolated from 293FT expressing TSPO WT, whereas no difference was observed with those isolated from 293FT expressing TSPO A/T Mut (Figure 2-4A, B). In particular, significant difference was observed between TSPO WT and A/T Mut in [^{18}F]fm-PBR28-*d2* uptake with 100 μg of membrane proteins (Figure 2-4C). Competitive inhibition assays were performed using [^{3}H]PK11195 on membrane proteins isolated from 293FT expressing TSPO WT and TSPO A/T Mut with unlabeled TSPO-targeting ligands. The ratios of IC_{50} values (TSPO A/T Mut/TSPO WT) showed 37.28 in fm-PBR28-*d2*, 1.14 in CB251 (Figure 2-5). These results reflected that fm-PBR28-d_2 ligand has a significant difference

in binding affinity according to TSPO polymorphism, whereas CB251 showed no difference in binding affinity according to TSPO polymorphism. This suggested that CB251 is a suitable TSPO-targeting ligand that goes beyond the limitation of 2nd generation TSPO ligands.

(A)

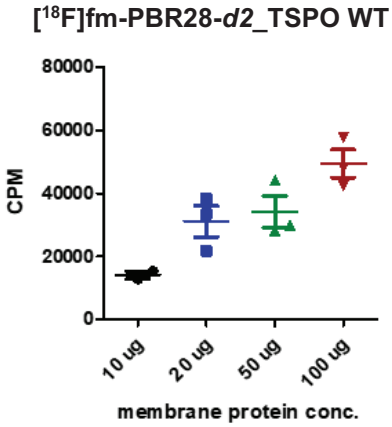
[18F]fm-PBR28-d2_TSPO WT
80000
60000
40000
20000
0
CPM
10 ug
20 ug
50 ug
100 ug
membrane protein conc.

(B)

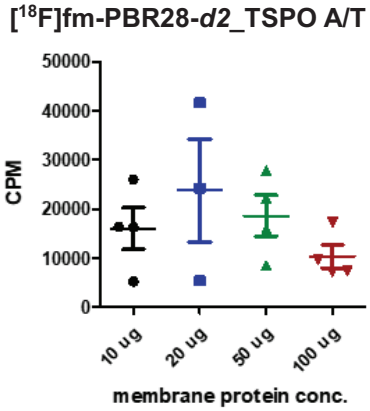
[18F]fm-PBR28-d2_TSPO A/T Mut
50000
40000
30000
20000
10000
0
CPM
10 ug
20 ug
50 ug
100 ug
membrane protein conc.

(C)

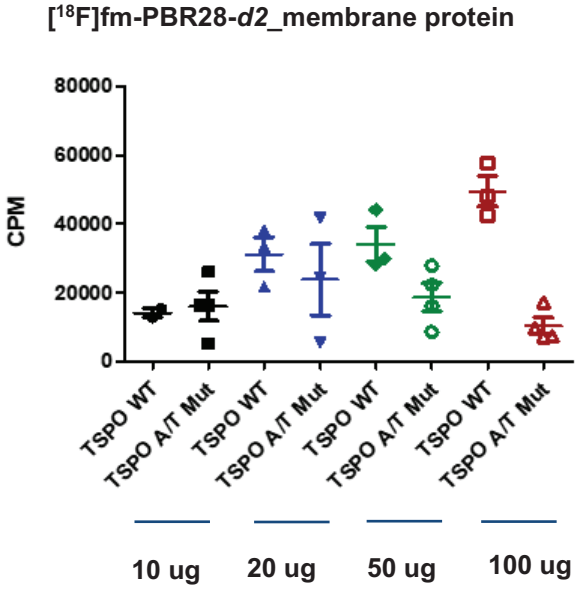
[18F]fm-PBR28-d2_membrane protein
80000
60000
40000
20000
0
CPM
TSPO WT
TSPO A/T Mut
TSPO WT
TSPO A/T Mut
TSPO WT
TSPO A/T Mut
TSPO WT
TSPO A/T Mut
10 ug
20 ug
50 ug
100 ug

Figure 2-4. Validation of membrane protein isolated from 293FT cells expressing TSPO WT or A/T Mut

(A) [^{18}F]fm-PBR-d_2 uptake in membrane protein isolated from 293FT cells expressing TSPO WT (B) [^{18}F]fm-PBR-d_2 uptake in membrane protein isolated from 293FT cells expressing TSPO A/T Mut (C) Graph of [^{18}F]fm-PBR-d_2 uptake according to concentration of membrane protein isolated from 293FT expressing TSPO WT or A/T Mut

(A)

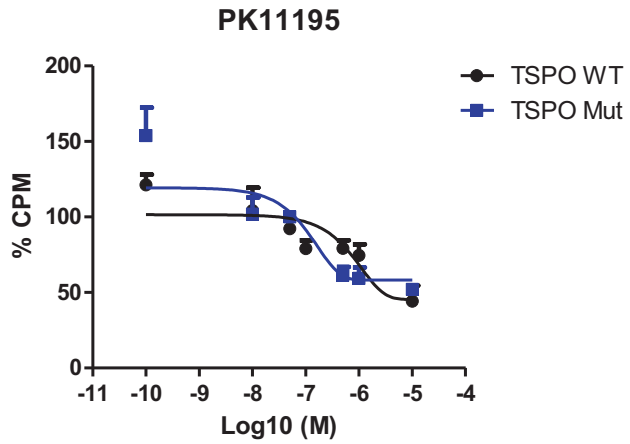
PK11195
TSPO WT
TSPO Mut
% CPM
200
150
100
50
0
-11
-10
-9
-8
-7
-6
-5
-4
Log10 (M)

(B)

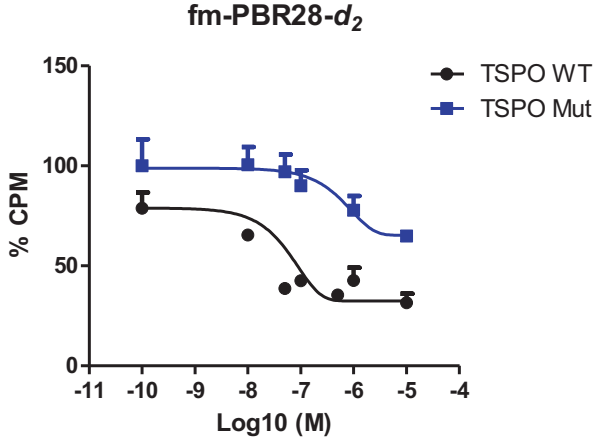
fm-PBR28-d_2
TSPO WT
TSPO Mut
% CPM
150
100
50
0
-11
-10
-9
-8
-7
-6
-5
-4
Log10 (M)

(C)

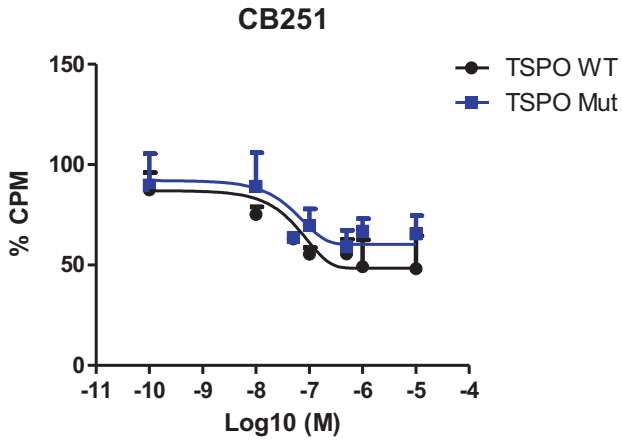
CB251
TSPO WT
TSPO Mut
% CPM
150
100
50
0
-11
-10
-9
-8
-7
-6
-5
-4
Log10 (M)

Figure 2-5. Competitive inhibition assay with [^{3}H]PK11195 using TSPO-targeting ligands in membrane proteins with TSPO WT and TSPO A/T Mut

(A) PK11195 precursor (B) Fluoromethyl-PBR28-d_2 (C) CB251

DISCUSSION

In chapter 2, I confirmed [^{18}F]CB251 was bound to the TSPO protein regardless of TSPO polymorphism by cell uptake of polymorphic TSPO expressing cells and competitive inhibition assay with polymorphic TSPO membrane protein. Vector systems for TSPO WT and TSPO A/T Mut were established. CB251 ligand showed similar uptake levels in cells with TSPO WT and A/T Mut. In addition, we determined and compared the IC_{50} ratio (TSPO A/T Mut/TSPO WT) of TSPO ligands by conducting competitive inhibition assay (Figure 2-5, Table 3).

Until now, several TSPO ligands have been developed for detecting neuroinflammation (Table 3). 2nd generation of TSPO ligands-PBR28, PBR111, DPA-713, XBD-173-overcoming the limitations by low binding affinity of 1st generation, showed promising results in preclinical studies (44, 50, 51). However, greater intra- and inter-variability in human has been reported as a major limitation.

The obstacle of [^{11}C]PBR28 as a commonly used TSPO-targeting PET probes in clinics is that the responder states are

divided into high affinity binder, mixed affinity binder and low affinity binder despite its high binding affinity to TSPO (47, 52). Thus, many chemists have been developed new TSPO PET probe with no difference in binding affinity according to TSPO polymorphism. CB251 ligand used in this study was verified by competitive inhibition assay that the binding affinity between TSPO WT and TSPO A/T Mut was similar (Figure 2-5). Since it has been reported that less than 3% of Asian have TSPO A147T mutant, it is difficult to obtain the samples from human. (http://asia.ensembl.org/Homo_sapiens/Variation/Explore?r=22:43162420-43163420;v=rs6971;vdb=variation;vf=210028659). Therefore, in chapter 2, I performed competitive inhibition assay with [^{3}H]PK11195 on membrane proteins isolated from 293FT cells expressing TSPO polymorphism. 293FT cells have basal expression of TSPO, therefore, it is difficult to find complete inhibition by A147T polymorphism in our results. However, the ratios of IC_{50} (IC_{50} A/T Mut/IC_{50} WT) was parallel to the reported Ki ratios (Ki LAB/Ki HAB) of TSPO ligands (47, 53).

In chapter 2, I assessed that [^{18}F]CB251 has the potential as a

suitable PET probe regardless of TSPO rs6971 polymorphism. I compared PK11195, a 1st generation ligand known as the gold standard TSPO ligand, and fm-PBR28-*d2,* a representative 2nd generation ligand with CB251. [^{18}F]CB251 uptake of cells with polymorphic TSPO showed similar uptake levels as cells with TSPO WT. It was confirmed by phantom study that these results were reflected in PET signal. In addition, IC_{50} ratio (WT/Mut) is closed to 1, indicating that binding affinity of CB251 is not affected by polymorphism. These results indicated [^{18}F]CB251 is a promising PET probe as polymorphism independent 3rd generation TSPO tracer.

REFERENCES

1. Calsolaro V, Edison P. Neuroinflammation in Alzheimer's disease: Current evidence and future directions. Alzheimers Dement. 2016;12(6):719-32.

2. Chen WW, Zhang X, Huang WJ. Role of neuroinflammation in neurodegenerative diseases (Review). Mol Med Rep. 2016;13(4):3391-6.

3. Thelin EP, Tajsic T, Zeiler FA, Menon DK, Hutchinson PJA, Carpenter KLH, et al. Monitoring the neuroinflammatory response following acute brain injury. Front Neurol. 2017;8:351.

4. Shabab T, Khanabdali R, Moghadamtousi SZ, Kadir HA, Mohan G. Neuroinflammation pathways: a general review. Int J Neurosci. 2017;127(7):624-33.

5. Guerriero F, Sgarlata C, Francis M, Maurizi N, Faragli A, Perna S, et al. Neuroinflammation, immune system and Alzheimer disease: searching for the missing link. Aging Clin Exp Res. 2016.

6. Winkeler A, Boisgard R, Martin A, Tavitian B. Radioisotopic imaging of neuroinflammation. J Nucl Med. 2010;51(1):1-4.

7. Nakamura K, Tukatani Y, Kubo A, Hashimoto S, Terayama Y, Amano T, et al. The behavior of ^{99m}Tc-hexamethylpropyleneamineoxime (^{99m}Tc-HMPAO) in blood and brain. Eur J Nucl Med. 1989;15(2):100-7.

8. Jin AY, Tuor UI, Rushforth D, Filfil R, Kaur J, Ni F, et al. Magnetic resonance molecular imaging of post-stroke neuroinflammation with a P-selectin targeted iron oxide nanoparticle. Contrast Media Mol Imaging. 2009;4(6):305-11.

9. Jacobs AH, Tavitian B, consortium IN. Noninvasive molecular imaging of neuroinflammation. J Cereb Blood Flow Metab. 2012;32(7):1393-415.

10. Esposito G, Giovacchini G, Liow JS, Bhattacharjee AK, Greenstein D, Schapiro M, et al. Imaging neuroinflammation in

Alzheimer's disease with radiolabeled arachidonic acid and PET. J Nucl Med. 2008;49(9):1414-21.

11. Caravagna C, Jaouen A, Debarbieux F, Rougon G. Overview of Innovative Mouse Models for Imaging Neuroinflammation. Curr Protoc Mouse Biol. 2016;6(2):131-47.

12. Pulli B, Chen JW. Imaging neuroinflammation - from Bench to Bedside. J Clin Cell Immunol. 2014;5.

13. Wu C, Li F, Niu G, Chen X. PET imaging of inflammation biomarkers. Theranostics. 2013;3(7):448-66.

14. Garello F, Pagoto A, Arena F, Buffo A, Blasi F, Alberti D, et al. MRI visualization of neuroinflammation using VCAM-1 targeted paramagnetic micelles. Nanomedicine. 2018;14(7):2341-50.

15. Albrecht DS, Granziera C, Hooker JM, Loggia ML. In vivo imaging of human neuroinflammation. ACS Chem Neurosci. 2016;7(4):470-83.

16. Narayanaswami V, Dahl K, Bernard-Gauthier V, Josephson L, Cumming P, Vasdev N. Emerging PET radiotracers and targets for imaging of neuroinflammation in neurodegenerative diseases: Outlook beyond TSPO. Mol Imaging. 2018;17:1536012118792317.

17. Zheng J, Boisgard R, Siquier-Pernet K, Decaudin D, Dolle F, Tavitian B. Differential expression of the 18 kDa translocator protein (TSPO) by neoplastic and inflammatory cells in mouse tumors of breast cancer. Mol Pharm. 2011;8(3):823-32.

18. Kim T, Pae AN. Translocator protein (TSPO) ligands for the diagnosis or treatment of neurodegenerative diseases: a patent review (2010-2015; part 1). Expert Opin Ther Pat. 2016;26(11):1325-51.

19. Kim T, Pae AN. Translocator protein (TSPO) ligands for the diagnosis or treatment of neurodegenerative diseases: a patent review (2010 - 2015; part 2). Expert Opin Ther Pat. 2016;26(11):1353-66.

20. Perrone M, Moon BS, Park HS, Laquintana V, Jung JH, Cutrignelli A, et al. A novel PET imaging probe for the detection and monitoring of

translocator protein 18 kDa expression in pathological disorders. Sci Rep. 2016;6:20422.

21. Wang Y, Coughlin JM, Ma S, Endres CJ, Kassiou M, Sawa A, et al. Neuroimaging of translocator protein in patients with systemic lupus erythematosus: a pilot study using [11C]DPA-713 positron emission tomography. Lupus. 2016.

22. Herber DL, Mercer M, Roth LM, Symmonds K, Maloney J, Wilson N, et al. Microglial activation is required for Abeta clearance after intracranial injection of lipopolysaccharide in APP transgenic mice. J Neuroimmune Pharmacol. 2007;2(2):222-31.

23. Catorce MN, Gevorkian G. LPS-induced murine neuroinflammation model: Main features and suitability for pre-clinical assessment of Nutraceuticals. Curr Neuropharmacol. 2016;14(2):155-64.

24. Lowery RL, Majewska AK. Intracranial injection of adeno-associated viral vectors. J Vis Exp. 2010(45).

25. Ngen EJ, Wang L, Kato Y, Krishnamachary B, Zhu W, Gandhi N, et al. Imaging transplanted stem cells in real time using an MRI dual-contrast method. Sci Rep. 2015;5:13628.

26. Wang YY, Yang YX, Zhe H, He ZX, Zhou SF. Bardoxolone methyl (CDDO-Me) as a therapeutic agent: an update on its pharmacokinetic and pharmacodynamic properties. Drug Des Devel Ther. 2014;8:2075-88.

27. El-Ashmawy M, Delgado O, Cardentey A, Wright WE, Shay JW. CDDO-Me protects normal lung and breast epithelial cells but not cancer cells from radiation. PLoS One. 2014;9(12):e115600.

28. Song MG, Kang B, Jeon JY, Chang J, Lee S, Min CK, et al. In vivo imaging of differences in early donor cell proliferation in graft-versus-host disease hosts with different pre-conditioning doses. Mol Cells. 2012;33(1):79-86.

29. Lemasson B, Serduc R, Maisin C, Bouchet A, Coquery N, Robert P, et al. Monitoring blood-brain barrier status in a rat model of glioma receiving therapy: dual injection of low-molecular-weight and

macromolecular MR contrast media. Radiology. 2010;257(2):342-52.

30. Herborn CU, Honold E, Wolf M, Kemper J, Kinner S, Adam G, et al. Clinical safety and diagnostic value of the gadolinium chelate gadoterate meglumine (Gd-DOTA). Invest Radiol. 2007;42(1):58-62.

31. Ahmad R, Raina D, Meyer C, Kufe D. Triterpenoid CDDO-methyl ester inhibits the Janus-activated kinase-1 (JAK1)->signal transducer and activator of transcription-3 (STAT3) pathway by direct inhibition of JAK1 and STAT3. Cancer Res. 2008;68(8):2920-6.

32. Thimmulappa RK, Fuchs RJ, Malhotra D, Scollick C, Traore K, Bream JH, et al. Preclinical evaluation of targeting the Nrf2 pathway by triterpenoids (CDDO-Im and CDDO-Me) for protection from LPS-induced inflammatory response and reactive oxygen species in human peripheral blood mononuclear cells and neutrophils. Antioxid Redox Signal. 2007;9(11):1963-70.

33. Vannini N, Lorusso G, Cammarota R, Barberis M, Noonan DM, Sporn MB, et al. The synthetic oleanane triterpenoid, CDDO-methyl ester, is a potent antiangiogenic agent. Mol Cancer Ther. 2007;6(12 Pt 1):3139-46.

34. Buendia I, Michalska P, Navarro E, Gameiro I, Egea J, Leon R. Nrf2-ARE pathway: An emerging target against oxidative stress and neuroinflammation in neurodegenerative diseases. Pharmacol Ther. 2016;157:84-104.

35. Barrientos RM, Kitt MM, Watkins LR, Maier SF. Neuroinflammation in the normal aging hippocampus. Neuroscience. 2015;309:84-99.

36. Russo MV, McGavern DB. Inflammatory neuroprotection following traumatic brain injury. Science. 2016;353(6301):783-5.

37. Busche MA, Konnerth A. Impairments of neural circuit function in Alzheimer's disease. Philos Trans R Soc Lond B Biol Sci. 2016;371(1700).

38. Shimizu M, Ishikawa J, Yano Y, Hoshide S, Shimada K, Kario K.

The relationship between the morning blood pressure surge and low-grade inflammation on silent cerebral infarct and clinical stroke events. Atherosclerosis. 2011;219(1):316-21.

39. Tousoulis D, Kampoli AM, Papageorgiou N, Androulakis E, Antoniades C, Toutouzas K, et al. Pathophysiology of atherosclerosis: the role of inflammation. Curr Pharm Des. 2011;17(37):4089-110.

40. Kuntner C, Kesner AL, Bauer M, Kremslehner R, Wanek T, Mandler M, et al. Limitations of small animal PET imaging with [^{18}F]FDDNP and FDG for quantitative studies in a transgenic mouse model of Alzheimer's disease. Mol Imaging Biol. 2009;11(4):236-40.

41. Buscombe J. PET imaging of inflammation. Q J Nucl Med Mol Imaging. 2014.

42. Vivash L, O'Brien TJ. Imaging microglial activation with TSPO PET: Lighting up neurologic diseases? J Nucl Med. 2016;57(2):165-8.

43. Le Fur G, Guilloux F, Rufat P, Benavides J, Uzan A, Renault C, et al. Peripheral benzodiazepine binding sites: effect of PK11195, 1-(2-chlorophenyl)-N-methyl-(1-methylpropyl)-3 isoquinolinecarboxamide. II. In vivo studies. Life Sci. 1983;32(16):1849-56.

44. Su Z, Roncaroli F, Durrenberger PF, Coope DJ, Karabatsou K, Hinz R, et al. The 18-kDa mitochondrial translocator protein in human gliomas: an 11C-(R)PK11195 PET imaging and neuropathology study. J Nucl Med. 2015;56(4):512-7.

45. Chauveau F, Boutin H, Van Camp N, Dolle F, Tavitian B. Nuclear imaging of neuroinflammation: a comprehensive review of [^{11}C]PK11195 challengers. Eur J Nucl Med Mol Imaging. 2008;35(12):2304-19.

46. Mizrahi R, Rusjan PM, Kennedy J, Pollock B, Mulsant B, Suridjan I, et al. Translocator protein (18 kDa) polymorphism (rs6971) explains in-vivo brain binding affinity of the PET radioligand [(18)F]-FEPPA. J Cereb Blood Flow Metab. 2012;32(6):968-72.

47. Owen DR, Gunn RN, Rabiner EA, Bennacef I, Fujita M, Kreisl WC, et al. Mixed-affinity binding in humans with 18-kDa translocator protein

ligands. J Nucl Med. 2011;52(1):24-32.

48. Kreisl WC, Fujita M, Fujimura Y, Kimura N, Jenko KJ, Kannan P, et al. Comparison of [(11)C]-(R)-PK 11195 and [(11)C]PBR28, two radioligands for translocator protein (18 kDa) in human and monkey: Implications for positron emission tomographic imaging of this inflammation biomarker. Neuroimage. 2010;49(4):2924-32.

49. Moon BS, Jung JH, Park HS, Contino M, Denora N, Lee BC, et al. Preclinical comparison study between [(18)F]fluoromethyl-PBR28 and its deuterated analog in a rat model of neuroinflammation. Bioorg Med Chem Lett. 2018;28(17):2925-9.

50. Werry EL, Bright FM, Piguet O, Ittner LM, Halliday GM, Hodges JR, et al. Recent Developments in TSPO PET Imaging as A Biomarker of Neuroinflammation in Neurodegenerative Disorders. Int J Mol Sci. 2019;20(13).

51. Endres CJ, Pomper MG, James M, Uzuner O, Hammoud DA, Watkins CC, et al. Initial evaluation of 11C-DPA-713, a novel TSPO PET ligand, in humans. J Nucl Med. 2009;50(8):1276-82.

52. Owen DR, Yeo AJ, Gunn RN, Song K, Wadsworth G, Lewis A, et al. An 18-kDa translocator protein (TSPO) polymorphism explains differences in binding affinity of the PET radioligand PBR28. J Cereb Blood Flow Metab. 2012;32(1):1-5.

53. Owen DR, Howell OW, Tang SP, Wells LA, Bennacef I, Bergstrom M, et al. Two binding sites for [^{3}H]PBR28 in human brain: implications for TSPO PET imaging of neuroinflammation. J Cereb Blood Flow Metab. 2010;30(9):1608-18.

국문 초록

서론: 신경 염증은 퇴행성 뇌질환의 주요 위험요인이므로 신경 염증을 진단하기 위한 영상적 방법들이 개발되었다. 활성화된 면역세포에서 과발현 된다고 보고된 Translocator protein (TSPO)는 유망한 염증 진단 바이오마커 단백질로서 이것을 타겟으로 하는 다양한 PET 프로브들이 개발되고 있다. 하지만 TSPO 유전자의 단일염기 다형성 (single nucleotide polymorphism)에 의한 TSPO 리간드의 결합친화도 차이는 병리 판단의 주요한 제한점으로 보고되었다. 본 연구에서는 [^{18}F]CB251 프로브가 유전자다형성에 비의존적인 TSPO 표적 프로브임을 평가하고 급성 신경 염증 모델에서 [^{18}F]CB251 PET/MRI 와 발광영상을 활용하여 신경 염증을 영상화 하였다.

방법: [^{18}F]CB251 의 TSPO 다형성에 대한 결합친화도를 확인하기 위해 2 가지의 TSPO 유전자 (TSPO wildtype, TSPO A147T mutant)를 발현하는 293FT 세포를 확립하였다. 확립한 293FT 세포에서 막 단백질을 분리하여 [^{3}H]PK11195 와 TSPO 리간드-PK11195, fluoromethyl PBR28-*d2*, CB251-로 경쟁적 억제 결합 분석을 진행하였다. 또한 TSPO 다형성을 가지는 293FT 세포에서 [^{18}F]CB251 의 세포 섭취를 비교하였으며 PET 스캔을 통한 phantom study 도 진행되었다. [^{18}F]CB251 의 세포섭취가 TSPO

특이적 반응인지 확인하기 위해 TSPO 발현을 조절한 세포에서 [^{18}F]CB251 의 섭취를 수행하였다. 신경 염증 영상을 위해 LPS 를 마우스 두개골 내로 주입하여 급성 신경 염증 모델을 확립하였다. Gd-DOTA MRI 영상으로 혈관-뇌 장벽의 파괴와 면역세포의 침투를 분석하였다. 또한 말초면역세포의 뇌 침투 정도를 발광영상을 통해 분석하였다. 말초면역세포는 루시퍼레이즈를 발현하는 형질전환 마우스의 비장에서 분리되었으며 그것은 급성 신경 염증 모델로 정맥 내 투여되었다. 신경염증은 [^{18}F]CB251 PET/MRI 와 발광영상(BLI)을 통해 진단되었고, [^{18}F]CB251 PET 시스템으로 신경염증 정도를 평가할 수 있는지 확인하기 위해서 급성 신경 염증 모델에 항염증 제제를 투여한 후 [^{18}F]CB251 PET/MRI 영상을 획득하고 발광영상도 함께 얻었다.

결과: CB251 리간드의 IC_{50} ratio (TSPO A/T Mut/TSPO WT)는 1.14 로 1 에 가까운 값을 보였다. 또한 TSPO 다형성을 가진 세포에서 [^{18}F]fluoromethyl-PBR28-*d2* 와는 다르게 [^{18}F]CB251 은 비슷한 섭취 정도를 보였으며, 세포에서 TSPO 의 발현 정도에 따라서 섭취에서 차이를 보였다. 또한 활성화된 면역세포에서의 [^{18}F]CB251 섭취가 면역세포에서의 섭취보다 유의미하게 높음을 확인하였다. 급성 신경 염증 모델에서 [^{18}F]CB251 PET/MRI 영상을 통해 신경 염증 부위에서 약 1.48 배 높은 [^{18}F]CB251 의 신호를 확인하였다. 또한 같은 뇌 부위에서 루시퍼레이즈를 발현하는 말초

면역세포를 발광영상으로 확인하였다. 항염증 제제가 투여된 급성 신경 염증 모델 뇌에서의 [^{18}F]CB251 의 신호와 발광 신호를 정량적으로 분석함으로써 염증 반응 정도를 평가하였다.

결론: 본 결과는 [^{18}F]CB251 PET 이 TSPO 단백질에 TSPO 유전자다형성에 관계없이 높은 결합 선택성을 보이며 신경 염증을 감지할 수 있음을 나타내었다. 또한 본 연구에서는 [^{18}F]CB251 PET/MRI 와 BLI 영상을 통한 항염증 정도를 평가함으로써 [^{18}F]CB251 PET 신호가 신경염증의 진행 정도와 치료 효과를 평가하기에 유용한 방법이 될 수 있음을 시사한다.

주요어 : 신경염증, 전이체단백질, 단일염기 다형성,
[^{18}F]CB251 양전자단층촬영
학 번 : 2014-25054